Universidade de Aveiro Departamento de Química

2017

Mariana Rodrigues Ferreira da Silva

Bionanocompósitos activos e inteligentes para embalagem alimentar

Active and intelligent bionanocomposites for food packaging

Universidade de Aveiro

Departamento de Químicа

2017

Mariana Rodrigues Ferreira da Silva

Bionanocompósitos activos e inteligentes para embalagem alimentar

Active and intelligent bionanocomposites for food packaging

Dissertação apresentada à Universidade de Aveiro para cumprimento dos requisitos necessários à obtenção do grau de Mestre em Biotecnologia, realizada sob a orientação científica da Doutora Paula Celeste da Silva Ferreira, Equiparada a Investigadora Coordenadora do Departamento de Engenharia de Materiais e Cerâmica da Universidade de Aveiro e da Doutora Cláudia Sofia Cordeiro Nunes, Pós-Doutoranda do Departamento de Engenharia de Materiais e Cerâmica da Universidade de Aveiro

This work was developed within the scope of project CICECO-Aveiro Institute of Materials, POCI-01-0145-FEDER-007679 (FCT Ref. UID/CTM/50011/2013).

This was work was financed by national founds through the FCT/MEC and when appropriate co-financed by FEDER under the PT2020 Partnership Agreement.

Júri

Presidente	Professor Doutor João Filipe Colardelle da Luz Mano professor catedrático do Departamento de Química da Universidade de Aveiro
Arguente	Professora Doutora Maria Elisabete Jorge Vieira professora auxiliar do Departamento de Engenharia de Materiais e Cerâmica da universidade de Aveiro
Orientadora	Doutora Paula Celeste da Silva Ferreira equiparada a investigadora coordenadora do Departamento de Engenharia de Materiais e Cerâmica da Universidade de Aveiro

Acknowledgements

Firstly, I would like to thank my supervisors Dr. Paula Ferreira and Dr. Cláudia Nunes for all the help provided and for their positivity, which was greatly appreciated, since I've been told (more than once) that I can be a little pessimistic.

I would like to thank: Dr. Rosário Soares from *Laboratório Central de Análises* of University of Aveiro for her support in XRD, Eng. Marta Ferro for help in SEM and TEM, Eng. Célia Miranda for her help providing data in DTA/TGA and BET analyses, both from the Department of Materials and Ceramic Engineering of University of Aveiro, and lastly but not least I would like to thank MSc. Celeste Azevedo from the Chemical Department of University of Aveiro for her help with Raman and UV-vis analyses.

I'm thankful for my lab colleagues namely for their help and camaraderie: Ana (thanks for answering my questions, I'm aware I've asked a lot of them), Joana, Zélia, Manuel, Mirtha, Idalina, Diana, Sara, Rita, Cátia and Alfredo.

And most importantly I would like to thank:

- My parents as cliché as the saying is, it is true - I wouldn't trade you for the world. I love you guys.
- My friends, you make my life better;
- My family thanks for always being there for me (special shout-out to my aunt Amélia not only for her remarkable exercise in patience and kindness but also for being one of the best people I have ever met);

Palavras-chave Dióxido de titânio, nanopartículas, hidrotermal, quitosana, compostos fenólicos, antocianinas, filmes.

Resumo

A produção de plásticos, baseados no uso de combustíveis fósseis, está a aumentar e estima-se que esta tendência continuará no futuro com impactos ambientais consideráveis. Os bioplásticos são uma alternativa amiga do ambiente. Biopolímeros como quitosana já foram adotados com sucesso para produzir bioplásticos que agem como substitutos do plástico em embalagem.

A quitosana foi selecionada devido às suas numerosas vantagens para embalagem alimentar, principalmente devido às suas atividades antioxidantes e antimicrobiana. Por outro lado, o dióxido de titânio foi selecionado como aditivo devido à sua capacidade de retirar oxigénio do ambiente e devido à possibilidade de poder ser facilmente funcionalizado para a formação de um sensor. Isto permitiria a formação de uma embalagem ativa e inteligente na proteção do alimento. Assim, nanopartículas homogéneas arredondadas e monofásicas de anatase de dióxido de titânio (TiO_2) foram usadas para melhorar os filmes de quitosana, criando um bionanocompósito. Estas nanopartículas de TiO_2 foram produzidas por síntese hidrotermal, tendo sido otimizadas as condições de síntese, como a temperatura e tempo, para selecionar as condições que originam as nanopartículas com as caraterísticas desejadas. As condições escolhidas para a produção do TiO_2 foram 200 ºC e 2,5 h devido ao tamanho, dispersão e tipo de nanoparticulas de TiO_2 produzidas. Os filmes de quitosana foram preparados com cerca de 9 mg de nanopartículas de TiO_2.

Para criar uma embalagem ativa e inteligente compostos fenólicos (principalmente antocianinas) de arroz preto (*Oryza sativa L. Indica*) foram adicionados para funcionalizar o TiO_2 (4,1 mg de extrato por filme).

Os filmes foram caracterizados em relação à sua atividade antioxidante, humidade, solubilidade, hidrofobicidade da superfície e propriedades mecânicas. Os melhores resultados foram obtidos nos filmes com nanopartículas e compostos fenólicos e foi demonstrado que a forma como cada componente é adicionado altera as suas propriedades. Os melhores resultados foram o aumento da atividade antioxidante, diminuição da solubilidade e da elasticidade, elongação e resistência à tração no filme composto por pigmento e TiO_2,. No entanto nestes últimos três parâmetros, a sua diminuição pode ser um aspeto positivo ou negativo dependendo das propriedades desejadas para o filme e o produto alimentar a embalar.

Keywords Titanium dioxide, nanoparticles, hydrothermal, chitosan, phenolic compounds, anthocyanins, films.

Abstract

Plastic production based in fossil fuels is rising, and predictions supports it continuous and enhanced use, with consequent environmental damage. Bioplastics are an environmentally friendly alternative. Biopolymers as chitosan have already been successfully used to produce bioplastics that act as plastic substitutes in packaging.

Chitosan was chosen for its numerous advantages for food packaging namely due to its antioxidant and antimicrobial activities. On the other hand, TiO_2 was selected due to its oxygen scavenging ability and due to its possibility to be easily functionalised to create a sensor. This would allow the construction of an active and intelligent packaging for food protection. Thus, monophasic anatase homogeneous round-shaped nanoparticles of titanium dioxide (TiO_2) were used as filler to improve the chitosan films, creating a bionanocomposite. These TiO_2 nanoparticles were produced via a hydrothermal method and its synthesis was optimized testing various reaction times and temperatures to find the conditions that create TiO_2 nanoparticles with the desired features. The conditions used for the chosen TiO_2 were 200 ºC and 2.5 h due to the size, dispersion and TiO_2 of the nanoparticles produced. The chitosan films were prepared with about 9 mg of TiO_2 nanoparticles.

To develop an active and intelligent food packaging, phenolic compounds (mainly anthocyanins) from black rice (*Oryza sativa L. Indica*) were used to functionalise the TiO_2 (4.1 mg of extract in each film).

The films were characterised regarding its antioxidant activity, humidity, solubility, surface hydrophilicity and mechanical properties. The best results were from films with both nanoparticles and phenolic compounds, and it was established that the order in which they are added alters its properties. The more notable improvements are an increase in antioxidant activity and a decrease in solubility, elasticity, elongation and tensile strength in the film containing pigment and TiO_2. However, the reduction of the later three properties can either be positive or negative, it depends on desired properties for the film for a chosen food product.

.

Table of Contents

Index of figures

Index of tables

List of symbols

A_{BET}	Specific surface area (measured by BET)
D_{SEM}	Average nanoparticles size (measured by SEM)
D_{TEM}	Average nanoparticles size (measured by TEM)
D_{XRD}	Average crystallite size in X-ray diffraction

Abbreviations

a.u.	Arbitrary units
BET	Brunauer-Emmet-Teller
BHA	Butylated hydroxyanisole
BHT	Butylated hydroxytoluene
COD	Chemical oxygen demand
DC	Direct current
DSSC	Dye-sensitive solar cells
DTA	Differential Thermal Analysis
EFSA	European Food Safety Authority
PHA	Poly(hydroxyalkanoate)
PLA	Poly(lactic acid)
ROS	Reactive oxygen species
SEM	Scanning electron microscopy
TEM	Transmission electron microscopy
TiO_2	Titanium dioxide
TGA	Thermogravimetric analysis
TTIP	Titanium tetraisopropoxide
UV-Vis	Ultraviolet and visible
XRD	X-ray Diffraction
ZnO	Zinc oxide

Chapter 1

1.1 Objective

The emerging need of moving towards biodegradable plastics made from renewable resources, as well as to improve food safety and security by implementing nanotechnologies to design intelligent and active food packaging, is the driving force for this Master thesis in Biotechnology. In this work, the main objective is to develop competitive active and intelligent biopolymer-based composite films for food packaging application.

The strategy to achieve the packaging material encompasses 4 main steps: i) preparation of TiO_2 particles; ii) extraction and quantification of phenolic compounds of black rice; and iii) preparation and full characterisation of chitosan-based composite films integrating the TiO_2 particles and the extracted phenolic compounds; and iv) preliminary testing of the bioplastic composite as anti-oxidant.

1.2 Structure of the thesis

The content of the thesis is divided in 6 chapters. The following chapter, chapter 2, is dedicated to the introduction of the material properties and State of Art. The experimental procedure and materials are described in chapter 3. Chapter 4 is about the particles synthesis and characterisation, so that the protocol can be refined to achieve the desired characteristics. The following chapter, chapter 5, is about films synthesis and characterization. In the 6^{th} and closing chapter, conclusions and future work are presented.

Chapter 2 Introduction

Nowadays everyone interacts with a wide variety of plastics. Plastics are used in packaging, office supplies, children's toys, gym equipment and manifold other products. The food packaging industry, in particular, heavily relies on its use. Plastic has been used in that industry since mid-20th century, mainly because of their low cost, good physicochemical properties, being easy to produce and use in large scale and it is aesthetically pleasant [1].

Every year about 300 million tons of plastic are made and this production accounts for 4% of the total global fossil fuel consumption. Even though 4% appears to be a small number it still pertains to tons of fossil fuel use, and moreover this number is on the rise and is expected that, in 2050, plastic production represent 20% of non-renewable fuels expenditure [2].

Fossil fuels are considered non-renewable since their use greatly outweighs its production. Fuels extraction and burning contribute to global warming by increasing the amount of greenhouse gases in the atmosphere. Additionally, the increase of atmospheric CO_2 also reduces water pH levels disturbing sea life [3]. On the other hand, several environmental issues arise as consequence of the non-biodegradability of plastics. Plastic waste is widespread, with extensive accumulation in oceans, landfills and other terrestrial compartments, affecting wildlife and possibly human health. In oceans, plastic products and debris are fragmented into smaller pieces and microplastics, which are then ingested and/or trapped by marine organisms [3]. Huge quantities of plastics are disposed in the environment, being extremely persistent, independently of their single or short-term use [4, 5].

For all of the aforementioned problems a need for alternative polymers that are biodegradable and/or made from renewable resources, ideally both, emerged [6]. Biopolymers can be found in animals (hydrocarbons, proteins, fats, nucleic acids, etc.), plants (e.g. cellulose, oils, starch, even polyesters) as well as in lower organisms [7].

Proteins and polysaccharides are the biopolymers of prime interest because they can be used effectively to make biodegradable films that can replace short shelf-life plastics [8]. It is therefore necessary to understand and improve these films to enhance and broaden its applications, turning them into viable alternatives to synthetic plastics. Additionally, it is also possible to improve the packaging materials with other functional capabilities such as to use components that actively react upon certain stimuli protecting food and enhancing its shelf-life. Another possibility is to use materials that can detect the food conditions and inform the consumer (intelligent packaging) [9].

2.1. Food packaging

Packaging materials play a very important role in maintaining food quality and safety during the products life cycle. A good packaging material should have good mechanical, thermal and

optical properties, resist to microbial growth and prevent contamination by hindering loss or gain of moisture (vapour barrier), prevent the permeation of undesirable gases such as oxygen, carbon dioxide or even volatile compounds that could change flavour and/or taste of the food stuff [10–13] Those characteristics make for a superior product all around but some properties can and should be added. The ideal packaging has all the aforementioned properties, but it should also be environmentally friendly by being biodegradable and made from bio-resources (Figure 2.1).

Several attempts have been made to create different packaging materials needed for each foodstuff. From the many materials explored, biopolymers in particular, show promising abilities.

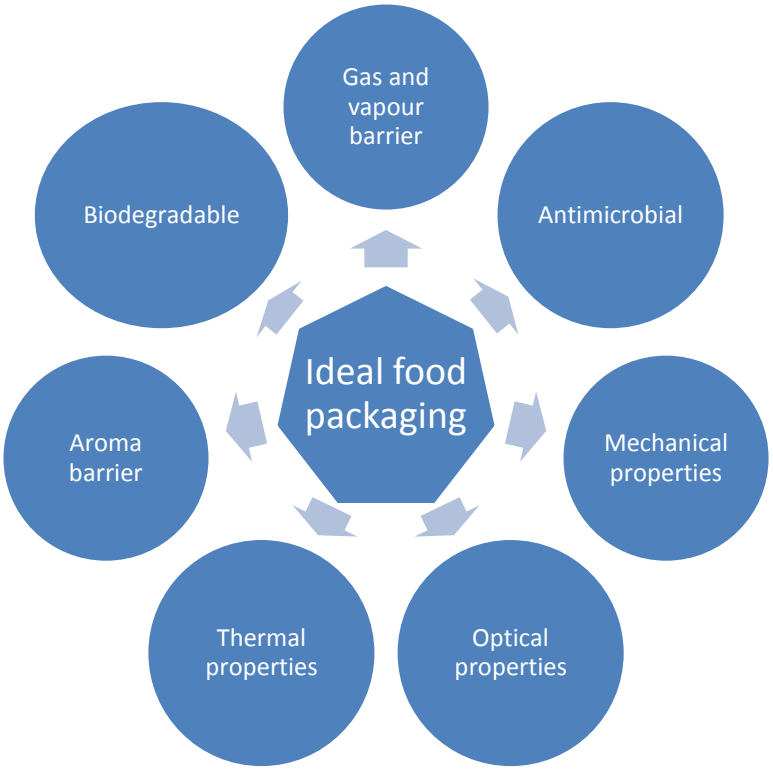

Figure 2.1- Ideal properties for food packaging.

2.2. Biopolymers

Biopolymers refer to polymers that are biobased and/or biodegradable [14]. A biodegradable polymer is a polymer that can be broken down into lower molecular products by cell (human, animal, fungi, etc.) activity, through an enzymatic process, although it is usually accompanied and promoted by physicochemical phenomena as well. The two types of processes, i.e. physic and

enzymatic, cannot be distinguished and/or separated, in general, and their combined effect leads to the complete degradation of the polymer.

In order to evaluate the polymers ability to be biodegraded, lab tests are used either based on the measurement of oxygen demand or on the amount of carbon dioxide involved in the process. This evaluation of biodegradability of polymeric materials is well defined in European standards [14].

Biopolymers can be divided, according to their sources, into artificial (bioplastics) or in natural polymers [7].

2.2.1. Natural polymers

Natural polymers occur in nature as macromolecules that can also be physically or chemically modified. They can be produced in complex metabolic processes, involving polymerization and enzymatic catalysis in cells of living organisms. These natural polymers are biodegradable, since they are created by metabolic processes in nature, they can be decomposed in that same environment [14]. Normally, the decomposing of these polymers releases the energy that they stored allowing its reuse. Natural biopolymers can include polysaccharides (such as cellulose, starch, and chitin), proteins (such as wheat gluten, soy, and glycerol), polyesters (polyhydroxyalkanoate, PHA, and polylactic-acid, PLA) [15]. One of the most used are polysaccharides due to their low cost and accessibility.

Chitin and chitosan

Chitin is the second most abundant polysaccharide in nature. Chitosan, known as soluble chitin, is a natural product obtained from alkaline deacetylated chitin [16] and is a potential renewable-resource-based plastic alternative. Chitosan is a linear polysaccharide of 2-amido-2-deoxy-β-D-glucoses attached by β(1→4) links (Figure 2.2) with a deacetilation percentage superior to 50% [17]. Chitosan molecular weight depends on its source and can vary from 100 to 1100 kDa and its deacetylation percentage can be between 50 and 90% [18]. Manipulation of deacetylation percentages allows tailoring its physicochemical properties and degradation profile [19]. Chitin can be retrieved mainly from the exoskeleton of marine crustaceans,[19] from fungal cell walls of *Aspergillus fumigares* and *Histoplasma farciminosum* and from the yeast *Saccharomyces cerevisiae* [20, 21].

Chitosan has an amino group (NH_2) that can be protonated to NH_3^+, and readily forms electrostatic interactions with anionic groups in an acidic environment. This amino group also

allows the incorporation of a variety of chemical groups, enabling its range of properties to be extended [22], allowing the prepared systems to react to external stimuli [23].

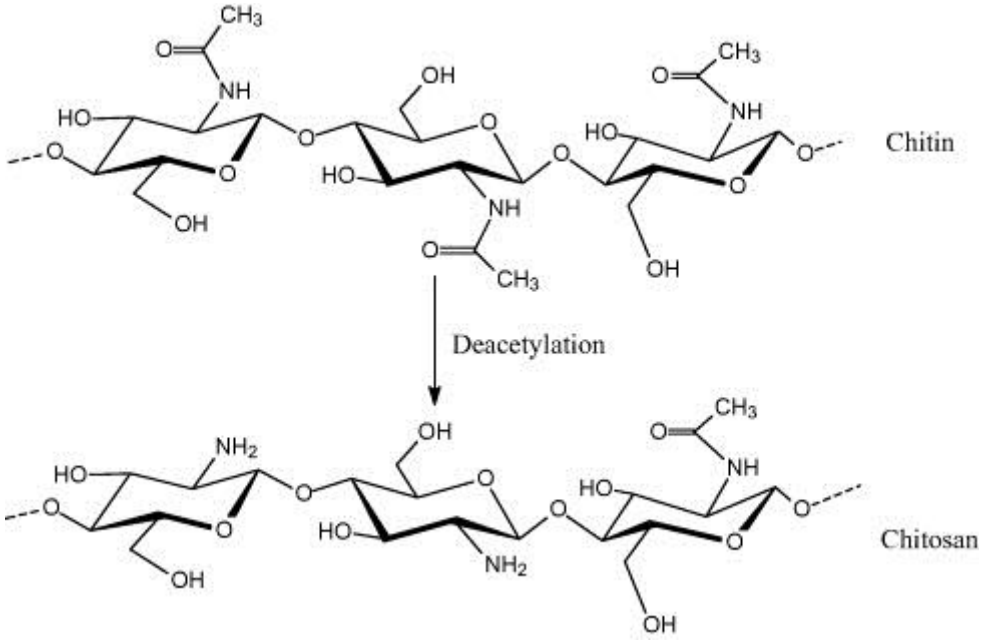

Figure 2.2. - Chitin and chitosan structures.[24]

This biopolymer has been widely studied for its potential use in areas such as biotechnology, material science[25], and pharmacology [26] because it can be obtained at low cost; has large scale availability; is non-toxic; biodegradable [19]; and has antifungal, antibacterial and antioxidant activities [27]. Those attributes create a material that protects food, mainly from fungal decay and can modify its atmosphere decreasing ripening and transpiration rates of fresh fruits [15]. These films are clear, tough, flexible and good oxygen barriers [15, 28]. However, they have weaknesses namely their lack of long-term stability and low water vapour barrier characteristics.

Chitosan antimicrobial activity depends on several factors, namely the origin of chitosan, molecular weight, degree of deacetylation, target organism, and conditions of the medium (pH, ionic strength, solutes that could interact with the active amine group of chitosan) [16]. It is, however, widely recognised that the most sensitive groups to chitosan are yeasts and moulds followed by Gram-positive and Gram-negative bacteria [16].

Regarding the effect of the molecular weight, it was found that chitosan of lower molecular weight (averaging less than 10 kDa) shows greater antimicrobial activity than chitosan of high molecular weight [29]. It is known that high solubility and charge density are fundamental for antimicrobial effect, so a possible explanation is that the low molecular weight chitosan is more soluble. The increased solubility facilitates the accessibility of the chitosan to the active sites of the target microorganisms enhancing antimicrobial activity rates [16].

The pH level can, if it is low enough (under 5.5), increase antimicrobial activity and provide a hurdle effect which contributes to increase bacterial stress [16]. A well-recognized theory, but not completely proven, is that the effect of pH levels, when under 6.3 (the pKa of chitosan), allow the positives charges of the amine group (NH_3^+) to interact with the cellular membranes, which are negatively charged. This results in leakage of intracellular components [30]. Another theory is that the cationic nature of this polysaccharide binds to bacterial cell walls through electrostatic interactions and disrupts its transport system for solutes or nutrients [16]. Additionally it is also possible that the charged amino group can bind to metals or metal complexes present in the medium [31] making them unavailable to the microorganisms metabolism, impairing their survival and/or growth.

The degree of deacetylation is also very important, a high amount of deacetylated amino groups results in more free amino groups to be protonated at low pH. This polymer requires a degree of polymerisation of at least seven glucosamine for it to have any antibacterial and/or antifungal activity.

Chitosan antioxidant activity is important because oxidation is a major problem affecting the food quality. Currently, the most frequently used antioxidants in active packaging are butylated hydroxyanisole (BHA) and butylated hydroxytoluene (BHT). These synthetic antioxidants although efficient and used in active food packaging (because of high stability, low cost and efficiency), have significant concerns regarding their toxicological aspects. Moreover, use of synthetic antioxidants is under strict regulation due to potential health risks. Therefore, extensive research has been conducted to employ some natural antioxidants such as phenolic compounds as alternatives to synthetic antioxidants as well as the use of natural antioxidant biopolymers (such as chitosan) [32]. Chitosan antioxidant activity, mainly chitooligomers, has shown a significant scavenging capacity against different reactive oxygen species (ROS). Its activity is even comparable to those obtained for commercial antioxidants, such as Trolox (6- hydroxy-2,5,7,8-tetramethylchroman-2-carboxylic acid) [33].

This antioxidant ability, both in chitosan and chitooligomers, is due the action of the amino group. As aforementioned when in acidic conditions, the nitrogen in the amino group receives a proton forming an ammonium group (NH_3^+), consequently its hydrogen ion can react with free radicals forming a stable molecule with oxidative ability [34]. Chitosan can also scavenge free radicals by donating a lone pair of electrons [35].

2.2.2. Strategies to enhance natural polymer properties

Natural biopolymers have drawbacks such as poor mechanical (brittleness), thermal (low heat distortion temperature) and barrier properties (high gas and vapour permeability), which compromises their use as food packaging materials [1, 32]. In order to improve natural biopolymers characteristics, different strategies can be employed, namely addition of plasticisers, other polymers (to form blends), molecules (to reticulate the polymers), and other fillers, creating biocomposites.

The use of plasticisers such as glycerol, ethylene glycol, and propylene glycol can be used to increase the flexibility, reducing brittleness and to improve processing. However, some of these compounds, such as ethylene glycol and propylene glycol, can be considered cytotoxic [37]. Plasticisers are usually used in conjunction with other approaches.

Making blends of biopolymers with other polymers allows the creation of materials with "tailor-made" properties (functional properties and at least a certain degree of biodegradability). Also, the incorporation of relatively low cost natural biopolymers into synthetic polymers provides a way to reduce the overall cost of the material and offers a method of modifying both properties and degradation degree [15].

Another alternative is the implementation of cross-linking agents that, through chemical cross-linking processes (covalent bond), improve the physical properties of chitosan films, namely enhance its mechanical strength and chemical stability, as well as decrease aqueous permeability and solubility. All while maintaining the films biological properties [33]. Some of the most used cross-linking agents are formaldehyde, glutaraldehyde, triphosphates, and glycerol polyglycidyl ether (also a plasticizer). However, these compounds are also cytotoxic [37]. Consequently non-cytotoxic alternatives were searched upon, resulting in the adoption of genipin (a natural cross-linking agent). Two genipin molecules can link to chitosan via its amine group forming heterocyclic compounds. Genipin is obtained from its parent compound, geniposide, via enzymatic hydrolysis with β-glucosidase. The compound is isolated from the fruits and flowers of *Genipa Americana* and *Gardenia jasminoides Ellis* [38].

Genipin has already been successfully used to improve chitosan films properties. In 2013, *Nunes et al*.[33] reticulated chitosan films with genipin and grafted with caffeic acid, resulting in a decrease in its solubility coupled with an 80% increase in its antioxidant ability.

Cross-linking can change properties but simple covalent bonds can also change properties although not always in a positive way, since it can disrupt the films matrix and interfere with mechanical properties. An example of compounds covalently linked to chitosan is phenolic compounds from wine (such as anthocyanins among others). They were covalently linked to

chitosan via its carbon 2 or 3 of glycosamine residues, which along with a cross-linking with genipin and using glycerol as plasticiser showed, in its best results, a decreased in solubility (mainly owed to genipin and to the hydrophobic behaviour of anthocyanins) and increase of antioxidant ability, of around 80%, due to the presence phenolic compounds [39].

One of the most promising ways of improving natural biopolymers films is by using nanofillers within the biopolymer. This creates a new type of material called bionanocomposites.

2.3. Bionanocomposites

This new typology of material plays an important role in increasing competiveness of natural biopolymers. Nanofillers are particles sized under 100 nm in one or more dimensions. There are numerous types of organic and inorganic nanofillers. The latter can be made of metals (e.g. silver, copper), metal oxides (e.g. TiO_2, ZnO), clays (e.g. cloisite, sepiolite, montmorillonite) and carbon. The nanofillers can exhibit different shapes such as nanoparticles, nanofibrils, nanorods, nanotubes, and nanoplatelets.

Different nanofillers bring distinctive effects to the bionanocomposites. The type of filler, morphology, and concentrations allow for some different arrangement and functionalities of the composites [36]. For instance, nanoclays are the most commonly used nanofillers in the synthesis of polymer layered silicate nanocomposites. Also when using carbon as filler, several nanostructures are possible, including fullerene (bucky-balls), carbon nanotubes (single-wall and multi-wall), carbon nanofibers, carbon nanoparticles, and graphene nanosheets. These carbon structures have been investigated due to their excellent physicochemical, mechanical and electrical properties [40].

Typical improvements of the use of nanofillers are the better mechanical and barrier properties. The mechanical properties of bionanocomposites strongly depend on the amount of nanofiller used. The enhancement of the mechanical property can be explained by the rigidity provided by the nanofillers as well as, in some cases, the affinity between biopolymer and nanofiller [1]. The interfacial interactions mentioned lead to a more rigid bionanocomposite which also improves thermal properties [1]. The betterment of barrier properties i.e. the decrease on the permeability, is especially important in the enhancement of food shelf-life. The addition of nanofillers increases the effective path length for gases to cross through the bionanopolymer. The longest the pathway for the gas or vapour molecules to cross the film, the most difficult is their diffusion and their contact with the foodstuffs. Particular nanofillers can also provide additional features to the bionanopolymer, like antimicrobial activity, oxygen scavenger capacity and sensor possibilities. Nanofillers such as silver or ZnO nanoparticles provide antibacterial and antifungal

abilities to the material [36]. Oxygen scavenger properties can be found in titanium dioxide (TiO_2) under ultraviolet radiation. Its use can help reduce or maintain oxygen levels, which is important since oxygen can lead to food deterioration. This ability to manipulate the amount of oxygen in a closed packaged makes the package an active one [9]. The presence of oxygen can cause browning in fruits and vegetables. When in contact with fat it can provoke rancid flavours, odours and it can turn food stale. Furthermore it can make the product seem less appealing to customers by causing pigment changes [36].

Another use of bionanocomposites can be the creation of flexible sensors, achieved by functionalizing suitable nanofillers. These sensors are able to detect and inform about the presence of by-products of food spoilage adding therefore, a new function to the packaging material to protect consumers [41].

An option of nanofiller with multiple advantages, when added to biopolymers, is the TiO_2.

2.4. Nanoparticles of TiO_2

TiO_2 has a wide variety of applications in conventional areas (pigments and cosmetics) and in more functional areas such photo-electrochemical cells [42], dye-sensitive solar cells (DSSC) [43], lithium ion batteries [44], sensors [45], electron field transition [46], microwave absorbing material, biomimetic growth and biomedical treatments [47, 48]

TiO_2 has been one of the most studied semiconductors because it has high efficiency, good thermal and chemical stability. In addition, it is non-toxic and low-cost [49]. TiO_2 is an EFSA (European Food Safety Authority) approved food additive (E171) and it has been used in the packaging industry due to its favourable characteristics. In the last 5 years TiO_2 has been found in more than 3500 foods or drinks, mainly in chewing gums, cakes and pastries, and confectionary. There are no epidemiology studies available regarding possible associations with adverse health outcomes [50].

2.4.1. Types of TiO_2

TiO_2 appears in three crystalline polymorphs in nature: rutile, anatase and brookite as seen in Figure 2.3. Each crystallographic phase exhibits different physical properties, such as refractive index, chemical reactivity, and photochemical reactivity [51].

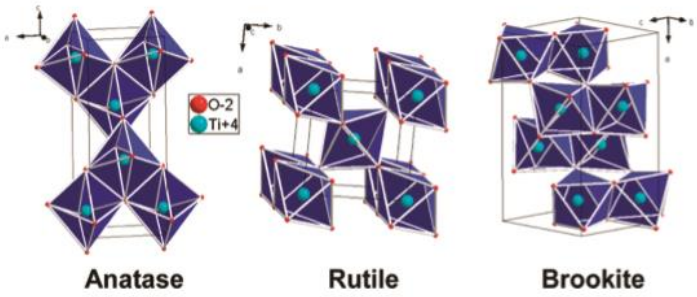

Figure 2.3. Representation of the TiO_2 anatase, rutile and brookite unit cells [52].

The stability of the polymorphs/phases depends on particle size. Anatase and brookite are metastable phases, difficult to synthesize and observe in pure forms, while rutile is the thermodynamically stable phase. Usually, anatase and brookite phases transfer, irreversibly, into rutile phase at high temperature (600 °C), nevertheless the specific temperature at which this transformation takes place depends on the preparation methods, precursors, and additives used in the particles syntheses [53]. Although rutile phase is thermodynamically stable, it is believed that anatase is the most active in photocatalysis, being the most intensely studied polymorph [49].

The difference between the polymorphs lies in the way their TiO_6^{-2} octahedral basic units connect. They share edges and corners in different orientation and distortions. Anatase forms from octahedra that share four edges. In brookite and rutile only three and two edges are shared, respectively [54, 55]. To distinguish between the three polymorphs, X-ray diffraction (XRD), Raman spectroscopy and transmission electron microscopy (TEM) are usually used.

To form a specific phase, the right precursor and pH level must be used, since they influence how the octahedral units assemble. At high pH, the high content of hydroxyl groups favours edge sharing, contributing for the formation of anatase. At low pH, more water molecules are bound to the positively charged Ti^{4+} centre. This favour corner sharing and the rutile phase formation [56].

The different crystallographic types of TiO_2 particles have facets [57]. Only in 2008, it was discovered that anatase crystals possessed promising properties associated with its {001} facet [58].

Certain ligands are known and used to expose particular facets so that the final product is further manipulated for specific uses. The choice of ligands plays a very important role in the structure and morphology of the final titanium oxide product [59].

2.4.2. Creating TiO_2 nanoparticles

There are many methods used for preparing TiO_2 nanoparticles. Those methods can be either physical or chemical. Physical methods usually consist of top-down approaches i.e. from raw material (visible at naked eye) to small-sized (nanoscaled). The advantage of this type of method is that it can usually produce large quantities of material. Top-down approaches have successfully fabricated highly uniform nanostructures and nanoparticles with controllable shapes and dimensions. For instance, Seungkyu Ha and his colleagues produced single-crystal TiO_2 with various nanoscale shapes, including cylinders, cones, and hourglass-shaped structures ranging from 100-600 nm in diameter and up to 1–2 μm in height. These structures were made by CHF_3-based and SF_6-based etching processes [60].

Chemical methods are usually a bottom-up approach, which uses molecular precursors (units) to form large structures. This type of method is typically performed at a small scale, therefore it is not used for industrial purposes like the physical approaches. The big advantage of this bottom-up method versus the top-down physical approach is that it allows for more precision in the material created. Due to the advantages that bottom-up approaches present, some of their methods will be the ones explored bellow for TiO_2 nanoparticle production.

2.4.3. General principles

The general principles of nanoparticles formation, in a bottom-up approach, in a solution-phase type synthesis occur in two events: nucleation and growth [49].

Nucleation is when nuclei are formed from the decomposition of the chosen precursor or by a sudden variation in the concentration of the reactive species. In both cases the concentration of precursors in solution reaches a supersaturating, which allows the nucleation event (Figure 2.4). For this reason the precursor used is important since it will determine the energetic pathway by which its monomers became active in the nuclei formation [49].

When the supersaturation decreases due to nuclei formation, the growth phase begins (Figure 2.4). In this phase no additional nuclei will be formed they will only grow to be larger clusters of monomers [61]. Growth can happen through two distinct mechanisms, monomer addition or Ostwald ripening. During monomer addition, the nuclei absorb the monomers, increasing its size. Ostwald ripening consists in making the smaller nanocrystals to be integrated by the larger particles. This process allows for a continuous process of size-focussing, which in turn makes for improved uniform particles [62]. In order to have uniform particles, other than having the Ostwald ripening mechanism, it is important that the nucleation stage happen in a very small time window,

meaning fast supersaturation followed by almost immediate nuclei formation. In this way the nuclei enter the growth phase all at the same time and all grow in similar conditions.

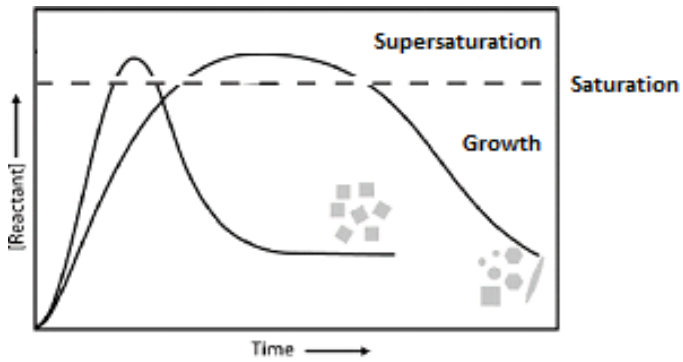

Figure 2.4 - La Mer model for nucleation and growth kinetics of nanoparticles (adapted) [49].

There are critical components for TiO_2 nanoparticles formation, namely some form of surfactants, protecting ligands, and the chosen metallic precursor. Some molecular species, such as ethanol, oleic acid, and benzyl alcohol, need to be used in order to prevent agglomeration of nanoparticles. This is possible by the introduction of steric and/or electrostatic interactions that keep the particles separated. Steric repulsion comes from the use of long-chain ligands or polymers with passive surface atoms, which results in reduced free surface energy that keeps the inorganic cores from fussing together. Electrostatic repulsion is obtained by forming an electrical double layer of ions around the nanoparticles, thus repulsing the charged particles [49].

The use of organic ligands or polymers that contain hydrolysable groups provide simultaneous steric and electrostatic stabilization. The most common organic functional groups used for this purpose are carboxylic acids, alcohols and diols, amines, phosphines, and phosphonic acids. The choice of a particular molecule is important to obtain the expected final product, because studies show that the ripening and particle orientation can be influenced by the adsorption of the ligand onto a particles specific facet [63]. Different ligands can also be used at various steps of the reaction in order to move the process forward. Distinct ligands have different binding strength and by substituting a molecule that binds to the inorganic core by another that binds to that same place but stronger, drives the nanoparticle syntheses process onwards.

There are several titanium precursors available. The main options are: titanium halides ($TiCl_4$, TiF_4 among others), titanatranes, titanium alkoxides ($Ti(OR)_4$), titanium(IV)bis(ammoniumlactato) dihydroxide ($(NH_4)_2(OH)_2Ti(C_3H_4O_3)_2$), titanium sulfate ($Ti(SO_4)_2$) and titanium oxysyulfate ($TiOSO_4$). Usually, the most used are alkoxides represented as $Ti(OR)_4$, where R represents an organic group. Titanium n-butoxide (R = $CH_2CH_2CH_2CH_3$), titanium *tert*-butoxide (R = $C(CH_3)_3$) and titanium isopropoxide or TTIP (R = $CH(CH_3)_2$) are mostly used. The latter was the one chosen as precursor in this work [64]. In alkoxides, the Ti(IV) centres are Lewis acids, being susceptible to

nucleophilic attack. This attack usually consists in a nucleophilic addition of water molecules onto the Ti(IV) centre followed by the transfer of hydrogen ions from water to the alkoxy groups. By control further the hydrolyses and the condensations, TiO_2 network can be created [49]. Since water is highly reactive with titanium alkoxides, the compounds must be handled with added attention to avoid excess humidity that would cause premature hydrolyses which would damage the TiO_2 synthesis.

Another important aspect are the methods employed, these also play a determinant role in the morphology and properties of the final products.

2.4.4. Methods for TiO_2 production

Within the chemical approach for TiO_2 synthesis exist three different categories: aqueous methods, nonaqueous methods and templated approach. Each of these categories has different methods (Figure 2.5).

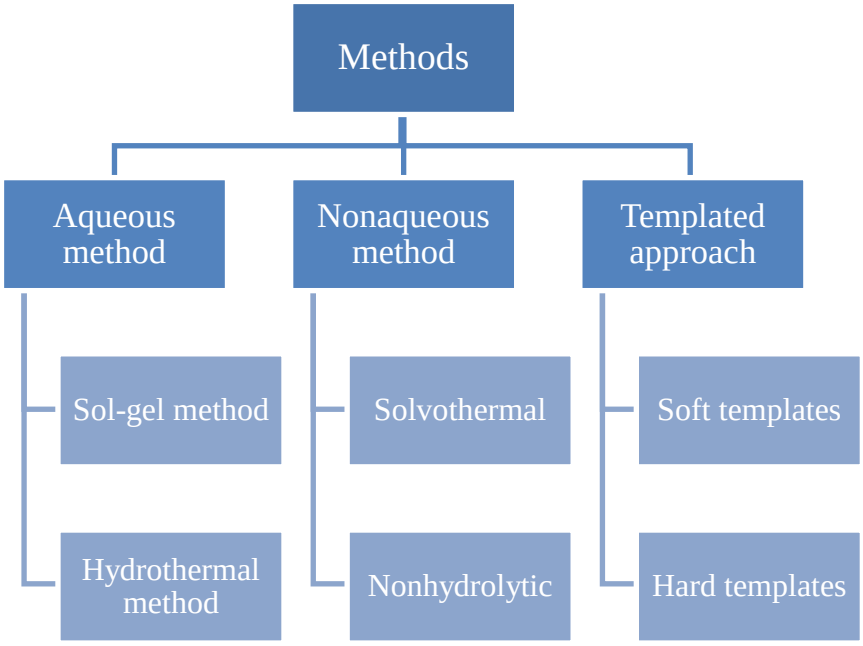

Figure 2.5. - Types of chemical TiO_2 synthesis.

Aqueous methods

The main used aqueous methods are the sol-gel and the hydrothermal methods.

When using aqueous methods for TiO_2 production, the main steps of the process are hydrolysis, condensation and polymerization. During hydrolysis, the titanium precursor suffers modification due to reaction with water. The condensation is the nucleophilic addition of the hydrolysed metal species forming Ti-O-Ti bonds. The condensation proceeds further until a metal oxide network is formed. At the same time water elimination is common in order to form the Ti-O-Ti bonds. The basic building unit consist of octahedral clusters where titanium atoms were coordinated to six oxygen species. These clusters share oxygen corners in a manner determined by the nature of the oxygen groups and by the presence of the chosen stabilizing molecules [49]. The morphology of the final particles depends on the poly-condensation direction determined by the different facets and on the capping agents action in the process [65].

In aqueous methods, the rates of aforementioned reactions can be altered either by using different pH or by using catalysts. Catalysts increase the speed at which the bonding network is formed. The catalysts can be acids or bases, promoting hydrolyses by dihydroxylation or deprotonation. [49]

Sol-gel method

The sol-gel method is widely used and involves the transformation of a sol (solution of colloidal particles) into a gel (metal-oxide tridimensional network). This gel then suffers a thermal treatment which allows the decomposition of the organic content resulting from solvents and, eventually, alkoxide precursors, followed by the formation of the desired final product [49].

The sol-gel method for TiO_2, specifically, can use both organic and inorganic precursors to form a gel that is usually transparent. The gel consists of a network of solid metal-oxygen bonds formed from precursors after chemical reactions and/or thermal treatments that exist in a liquid phase. This gel is then dried and transformed into TiO_2 by thermal treatment(s) [53].The disadvantages of this approach are the control of the kinetics of the hydrolyse and condensation reactions. The speed at which these reactions occur is extremely high, thus turning the control over shape, size and dispersion quite poor [49]. Additionally the precipitates are usually amorphous and require further heat treatment to induce crystallization [51]. However, the calcination process frequently gives rise to particle agglomeration and grain growth [66].

Hydrothermal method

Hydrothermal method allows to achieve crystalline materials at a temperature significantly lower than the required by sol-gel, however shape control and uniformity are still a challenge [49]. This method typically uses a base such as ammonia or an alkaline hydroxide in order to form a titanium hydroxide intermediate. The intermediate is then dehydrated to form TiO_2 under hydrothermal conditions at temperatures between 150 and 250 ºC using an autoclave container, which creates pressure under heating. In order to control size and shape, it is fundamental to use mineralizers to define the optimal pH, vary the temperature levels, as well as stirring speed, keeping similar solution volume quantities. The reaction time under said conditions is also an important factor; since it can be necessary go through metastable phases in order to reach the final desired morphology [49].

Non-aqueous methods

In non-aqueous methods, the TiO_2 reacts through mechanisms, which do not involve hydrolysis and condensation. Non-hydrolytic sol−gel describes reactions in which an oxide forms without any addition of water, through reactions with oxygen-containing organic molecules. For non-aqueous sol−gel processes, hydrolysis occurs through reactions with water produced *in situ*. The distinction between the two can be difficult leading to mistakes in literature [49, 53].

The mechanisms for TiO_2 production usually have three steps: i) alkyl halide or ether elimination by cross-reactions between different titanium precursors to form Ti−O−Ti bonds; ii) thermal decomposition of the organic part of the precursors and solvents; and iii) *in situ* formation of water (or another activated form of water), either by esterification or aminolysis through the reaction of a metal carboxylate precursor with an alcohol [67] or an amine [68]. As previously mentioned, it is difficult to distinguish between non-aqueous sol−gel and non-hydrolytic sol−gel because it is unclear whether water is produced or not during the reaction. The main advantage of non-aqueous approaches is the better control over reaction rates than in the case of aqueous methods (sol-gel and hydrothermal methods). When water is not present or is produced *in situ* in small quantity, hydrolysis and condensation occur slowly, offering a kinetic control of the hydrolysis reaction. Even more, it becomes possible the use surfactants and organic ligands which were insoluble in an aqueous medium. This increases the amount of substances available to adjust the precursor reactivity allowing for unprecedented control over the morphology of TiO_2 crystals and nanoparticles [49].

The two main approaches classified as non-aqueous methods are the solvothermal and the non-hydrolytic syntheses.

Solvothermal method

Solvothermal methods are conducted in an autoclave with non-aqueous primary solvents at elevated pressures, similarly to hydrothermal methods [49]. It is widely used to produce crystals with tailored facets, like the hydrothermal method, due to the versatility to manipulate nucleation and growth [57].Water is not used as a primary solvent but it can, sometimes, be added to induce hydrolysis [49].

Non-hydrolytic method

As opposed to the solvothermal method the non-aqueous surfactant-assisted protocols are conducted at, or near, atmospheric pressure. This process is based on reactions that yield the desired Ti−O−Ti bonds while using surfactants that participate both in the growth of TiO_2 and in the modulation of its facets [57]. An advantage of this type of synthesis is the modulation of the reactivity of the chosen titanium precursors using surfactant molecules, which act also as protecting agents.

Templated approaches

Templates or structuring directing agents can be used to define the morphology of TiO_2 nanoparticles [49]. They belong to two main categories: the soft and the hard templates.

Soft templates

Soft templates are formed from flexible organic or biological based molecules. They may form microemulsions or micelle arrangements. Microemulsions are thermodynamically stable dispersions in which amphiphilic surfactants (containing hydrophilic and hydrophobic parts) stabilize small droplets of one liquid within a second liquid in which it is immiscible. Alternatively, micelles are aggregates of surfactants that are formed in solution when the concentration of surfactant exceeds the critical micelle concentration (cmc) [49]. In the soft template approaches in order to produce TiO_2 particles, the droplets act as nanoscale reactors in which precursors are dissolved, needing to be stabilized by surfactants [69]. Usually alkoxides are the chosen precursors in microemulsions or swollen reverse micelles [49].

Hard templates

The hard templating uses rigid inorganic or polymeric materials as templates, which allow TiO_2 to be coated on the surface of a material forming shells. After that, the template can be dissolved or thermally decomposed [49].

2.4.5. Properties TiO_2

TiO_2 nanoparticles can be used as fillers in composites to improve mechanical and barrier properties by the mechanisms explained in the subchapter 2.3.

A notable aspect of the use of TiO_2 is the oxygen scavenger ability. Under UV light, nanocrystalline TiO_2 films, in the presence of excess of hole scavengers, can cause deoxygenation of closed environments. Under aerobic conditions, the oxygen reduction reaction is observed to exhibit first order kinetics with a rate constant of 70 s^{-1} from the reduction of oxygen by photogenerated TiO_2 electrons. The reaction steps can be summarised by the Equation 2.1. The development of an efficient light driven oxygen scavenging system would be novel approach to achieving anaerobic environments. These environments could be key in a wide range of applications, ranging from food packaging to organic electronics [70].

$$\text{Organic} + O_2 \xrightarrow[TiO_2]{h\nu \geq 3.2\ \text{eV}} CO_2 + H_2O$$

Equation 2.1 – Typical photocatalytic reaction [70].

Moreover, during these photocatalyzed chemical reactions, reactive oxygen species (ROS), including superoxide radicals ($O_2^{-\bullet}$) and singlet oxygen, as well as other intermediate species such as H_2O_2 or O_2 are also formed [71]. Due to those highly reactive free radicals generated during UV irradiation, engineered TiO_2 NPs have also been recognized for their light-induced biocidal effects against a broad range of harmful microorganisms, such as the bacteria *Escherichia coli* [72] and molds, like *Aspergillus niger* [73]. This is possible because ROS play critical roles in several physiological processes in living beings namely in the regulation of the immune system and in the development of the inflammatory response, activation of transcription factors and gene expression, and modulation of programmed cell death (i.e. apoptosis) [74]. Excessive levels of ROS can also oxidize cell constituents such as lipids, proteins, and DNA, and consequently pose a threat to cell integrity [75].

Thanks to titanium dioxides usefulness against photo-oxidation, due to its ability to scatter light and absorb UV light energy, it has been added at different concentrations to HDPE (High-density polyethylene) and PETE (Polyethylene terephthalate) as a light blocker [76]. It is also frequently used in sunscreen for protection, particularly, against UV-B radiation. The TiO_2 valence band possesses many densely packed electron states that allow many absorption possibilities, as long as the energy absorption exceeds the band gap width. That is partly why TiO_2 nanoparticles absorb more in the UV-B spectrum [77].

2.4.6. Sensors for food packaging

The functionalization of TiO_2 nanoparticles surface allows the creation of unique target sites for selected molecules. TiO_2 has been used in sensors because it can form coordination bonds with the amine and carboxyl groups of enzymes, maintaining the enzyme biocatalytic activity [78]. In addition, TiO_2 has the ability to harvest electrons produced by the reaction between certain (bio)molecule and an analyte. These electrons can then be transferred to an outer circuit, which detects the reaction.

The construction of these sensors will allow the packaging to become an intelligent one with systems capable of providing the consumer with information on the conditions of the food or its environment (temperature, pH) [9]. It is important to note that sensing purposes can only be achieved using TiO_2, which has been tailored for this application.
Titanium dioxide is mostly used for COD (chemical oxygen demand), gas, and other sensors [79].

2.5. Biogenic amine detection

One of the main adversaries to food safety are biogenic amines, such as tyramine, trimethylamine, 2-phenylethylamine, histamine, putrescine, cadaverine, among others. These amines result from the decarboxylation of amino acids in food (such as meat, fish, and milk) by bacteria (including pseudomonas and lactic acid bacteria) [80]. These amines are undesirable in food stuff because they are frequently involved in human pathologies such as: neurological disorders, gastrointestinal diseases, abnormal immune responses, cancer and are potentially toxic [81]. It is therefore understandable why a sensor for its detection would improve food safety and avoid potential health hazards for consumers.

There are several different approaches taken for amine detection based on different sensing mechanisms. These include electrochemical, mass, optical-based among other gas sensing methods. However, for packaging the best option is an optical-based sensor.

Even though many reports are available on the physical characterization of TiO_2 films and the different methods to produce it, the gas sensing properties of this promising material have not been explored in great amount [82]. This is even more glaring when searching for gas detection for biogenic amines. The better option found was made by pigment-sensitizing a thin layer of TiO_2. The TiO_2 film was deposited by a DC reactive magnetron sputtering technique onto a well-cleaned glass substrate equipped with interdigitated comb shaped electrodes. The natural pigments used to detect amines were extracted from spinach (*Spinacia oleracea*), red radish (*Raphanus sativus L*), winter jasmine (*Jasminum nudiflorum*), and black rice (*Oryza sativa L. indica*) using alcohol. The pigment displaying the best results was from black rice because it had the biggest amount of anthocyanin, promoting the strongest interaction between its carbonyl and hydroxyl groups the TiO_2 film. Anthocyanins (ATH) represent a large group of natural, water soluble, nontoxic pigments. They are polyphenolic plant pigments, responsible for the red, blue and purple colours of many fruits, vegetables and grains. They are most frequently glycosylated at the C3-position, followed by the C5- position. Glycosylation at C-7, C-3 or C-5 is often found. The colour of ATH changes depending on the pH, co-existing colourless compounds (co-pigments, typically flavones and flavonoids), storage temperature, chemical structure, concentration, light, oxygen, solvents and the presence of enzymes, proteins and metallic ions [83]. This pigment has successfully been used in biocomposites of chitosan and ATH to detect pH changes [83].

When ATH is used to functionalise TiO_2, relatively low humidity is necessary for sensing because water could promote pigment desorption from TiO_2. Darkness is also required, because light could cause the pigments degradation and as result decrease the sensor sensibility. This gas sensor works because, under amines gas condition, anthocyanin absorbs electrons from the amines (and injects electrons into the semiconductor conduction band). Therefore, the conductivity of the TiO_2 films correlates with the concentration of the amines. This sensor was used the detect amines during pork meat decomposition and the results were highly positively correlated with the content of cadaverine and putrescine [84]. Other works have been made with other natural pigments such as cyanidin and have achieved similar successful amine detection [85].

Colourimetric approaches have also been successfully used using natural pigments namely the aforementioned ATH. These type of sensors use colour to display pH changes in food that usually signify food decay. The following example uses ATH from red cabbage, chitosan and starch but not TiO_2 for amine detection; This study had good results namely: colour change at different pH levels while knowing that the extract was physically incorporated into the polymeric matrix, meaning that the chemical properties of the extract are not affected by the incorporation into the matrix. This is important information because until this point it was unknown if chemical

interaction between the polymeric matrix and the extract would affect the sensitivity of the extract to pH changes [86].

Another example of a colourimetric sensor was the work by Yoshida et al used anthocyanins in chitosan films resulting in the achievement of colour changing-pH dependent (as expected) and a reduced solubility with a slight interference in chitosans mechanical properties, namely a decrease in elongation at break [83].

Chapter 3 Experimental section

3.1. Particles production

The TiO_2 particles were made using the hydrothermal method. This method proceeds as follows: 10 mL ethanol (anhydrous, 99%, Carlo Erba) and 8 mL acetonitrile (anhydrous, 99.8%, Sigma-Aldrich) were mixed and 6.9 µL methylamine (40 wt% in H_2O, Aldrich) solution was added. Then, 1.20 mmol titanium(IV) isopropoxide or TTIP (97% trace metals basis, Aldrich) was dripped into ethanol (2 mL) and dissolved in the above solution with continuous magnetic stirring. Subsequently, 30 mL ethanol/H_2O (1:1) solution was added drop wise to the solution with stirring for 1 h. The mixture was transferred into a 100 mL Teflon-lined stain steel autoclave and kept at a set time and temperature in a lab oven. After cooling, the solution was centrifuged and washed with absolute ethanol and deionized water and stored in the latter.

Table 3.1 details the synthesis conditions of all particles. The samples were divided in series by the variable studied, i.e. the samples in the temperature series have different temperatures. All samples are designated with the following pattern: "temperature_# h", in which the value of temperature is presented in Celsius degree (°C) and # means number of reactions hours.

Table 3.1. Sample designation and synthesis conditions.

	Sample designation	**Temperature (ºC)**	**Time (h)**
Temperature series nr. 1	170_5h	170	5
	180_5h	180	5
	190_5h	190	5
	200_5h	200	5
	215_5h	215	5
	230_5h	230	5
Temperature series nr. 2	170_1h	170	1
	180_1h	180	1
	190_1h	190	1
	200_1h	200	1
	215_1h	215	1
	230_1h	230	1

Table 3.1. Continued

	Sample designation	Temperature (ºC)	Time (h)
Time series	200_1h	200	1
	200_2h	200	2
	200_2.5h	200	2.5
	200_3h	200	3
	200_4h	200	4
	200_5h	200	5

An amine series was also created to investigate its impact in TiO_2 particles formation. The series follows this designation: 200_5h_quantatity and type of amine used (M for methylamine and E for ethylamine). For instance, 200_5h_3xM, used triple the usual amount of methylamine (described above).

Table 3.2 - Sample designation and synthesis conditions of the amine series.

	Sample designation	Amine used	Amount used (µL)
Amine series	200_5h_none	-	0
	200_5h_ M	Methylamine	6.9
	200_5h_3xM	Methylamine	20.7
	200_5h_E	Ethylamine	6.9

3.2. Phenolic compounds extraction

The phenolic compounds were extracted from black rice (*Oryza sativa L. Indica*). The rice was blended (Blender CPE10 Model 39BL16, Cole-Palmer® Instrument Company) to a fine powder, which was then incubated for a minimum of 48 h in a lab oven at 60 ºC. The powder was subsequently immersed in absolute ethanol (anhydrous, 99%, Carlos Erba) for a week. The solids were filtrated out, and the filtrates were concentrated at 40 ºC in a vacuum rotary evaporator for further application in the films (Figure 5.2).

3.3. Phenolic compounds quantification

The method was carried out in a microplate. Then, 60 µL of water are put in the microplate followed by 15 µL of Folin-Ciocalteau reagent (Merck) and 15 µL of sample (diluted accordingly) or standard solution (for the calibration curve). These solutions are left to react for 5 min and then 150 µL of 7% Na_2CO_3 solution are added. The microplate is incubated at 30 ºC for 60 min, after which absorbance is measured at 760 nm in BioTek Eon™ spectrophotometer.
A solution of gallic acid (Fluka) of 0.250 mg/mL was prepared and used as standard to establish a calibration curve, which allows the determination of the amount of phenolic compounds in a sample. The concentrations made were (0.05, 0.1, 0.15, 0.2 and 0.25 mg/mL).

3.4. Films preparation

Table 3.3 - Chitosan- based films designations and components used in their preparation.

Film designation	**Components**
Film C	Chitosan
Film T	Chitosan and TiO_2 particles
Film P	Chitosan and Phenolic extract (Pigment)
Film TP	Chitosan, TiO_2 particles and Phenolic extract (fillers mixed together before addition to chitosan)
Film T+P	Chitosan, TiO_2 particles and Phenolic compounds (fillers added separately to chitosan)

Film C is a **c**hitosan-based film and is prepared to act as film control or blank (Table 3.3). A chitosan solution (medium molecular weight, 85% of deacetylation, Aldrich) 1.5 % (w/v) in an acid acetic solution 0.1 M (Aldrich, ≥ 99.7%) was made and left to agitate for 16 h at room temperature. After the chitosan was completely dissolved, the solution was filtrated in a Büchner funnel with a G1 glass filter. To the resulting solution it was added 0.25% (w/w) of glycerol (Fisher Chemicals, 98%), as a plasticizer. To promote better homogenization, the solution was heated at 50 ºC with stirring (in water) for 10 min. The next step was to distribute 31 g of the solution in acrylic plates of 144 cm^2. The plates were placed in an oven for 16 h at 35 ºC to allow solvent evaporation [87].

Film T is a chitosan film containing TiO_2 particles as filler (Table 3.3). The chitosan film followed the same steps as in film C, but before the glycerol addition, 0.02% (w/w) of 200_2.5h

particles were added. After the particles addition, the solution was stirred until it become homogenous. The glycerol was then added, and the film casting proceeds as described before.

The film denoted as P is a chitosan film containing the black rice extracted phenolic compounds (Table 3.3). The chitosan solution went through the same steps as in film C, but, before the glycerol addition, 0.9 % (w/w) of phenolic compounds was added. The phenolic compounds were added to the filtered chitosan solution and were stirred to form a homogenous mixture. The preparation proceeded as described before.

The film TP is formed by a chitosan matrix to which was added the TiO_2 particles previously reacted with the phenolic compounds (Table 3.3). The chitosan solution went through the same steps as in film C, but for film TP, before glycerol addition, the mixture of particles (0.02 % (w/w) with the phenolic compounds (0.9% (w/w) was added and homogenized. After filtration of the solution, the glycerol was introduced in the mixture and the procedure of Film C was followed.

The Film T+P is also formed by chitosan, TiO_2 particles and phenolic compounds (Table 3.3). The difference between this film and the Film TP is how TiO_2 particles and phenolic compounds are introduced to the chitosan solution. In the Film T+P the TiO_2 particles are added first, and after homogenization the phenolic compounds were added.

3.5. Structural and morphological characterization

3.5.1 X-Rays Diffraction (XRD)

X-ray diffraction was used for a qualitative and quantitative analysis of the TiO_2 crystallographic phases present in the samples. This technique is versatile and non-destructive. The XRD were performed using *Philips X-pert MDP* equipment with Cu-K_α X-radiation and λ=1.5406 Å. The sweeping angles used for identification of the crystalline phases in TiO_2 particles were from 20 to 80º with a step of 0.02º at room temperature. For phase identification through the X-ray diffraction peaks, an integrated database of *Powder Diffraction Files* (PDF) from the *International Centre of Data Diffraction* (ICDD) was used.

3.5.2. Scanning Electron Microscopy (SEM)

Scanning Electron Microscopy was used to reveal the microstructure of TiO_2 particles as well as their dispersion on the polymer matrix.

The SEM equipment used was Hitachi® model SU-70. This microscope can achieve magnifications from 30 to 800000 times with acceleration voltage in range 0.1 to 30 kV. The images were taken with magnifications from 5000 to 150000 times at 4 and15 kV.

For the samples preparation regarding the particles, they were kept suspended in water and that solution was dropped onto a platinum substrate and left to dry at room temperature overnight. The particles were also measured, from the resulting SEM images, assisted by the software ImageJ version 1.50i [88]**.** The average particle size of the SEM particles results from the analysis of around 100 particles. The films were stacked onto a typical SEM sample-holder with carbon tape and coated with carbon for the observation.

3.5.3. Transmission Electron Microscopy (TEM)

The TiO_2 particles were analysed by transmission electron microscopy (TEM) using a Hitachi® model H9000 microscope with an acceleration potential of 300 kV. The particles were suspended in water and a droplet of suspension was deposited onto a lacey carbon coated copper grid from Agar Scientific® and left to evaporate overnight at 35 ºC in a lab oven.

3.5.4. Specific Surface Area (A_{BET})

The -196 °C Nitrogen adsorption isotherm based on the Brunauer-Emmett-Teller (BET) was used to determine the specific surface area of powders or porous materials [89]. The equipment used was *Micromeritics® – Gemini 2380 V2.00*. N_2 was used as the adsorption gas and liquid N_2 was used to cool down the samples. The TiO_2 samples were degassed at 200 ºC overnight.

3.5.5. Differential Thermal (DTA) and Thermogravimetric Analysis (TGA)

Differential Thermal Analysis (DTA) is a technique based on the thermal behaviour, (heat gain or loss) due to structural changes in a material, as temperature increases. The thermogravimetric analysis (TGA) records weight loss of the sample upon temperature increase. The weight loss can be due to evaporation of water, solvents and organic matter decomposition with the release of carbon dioxide and water.

The titanium dioxide particles were analysed to know their thermal stability. The particles were in a water solution that was dried overnight at 70 ºC before thermal analyses. The equipment used was *Setaram™* model *Labsys TG-DSC16.* The analyses were performed by heating the powder from room temperature up to 800 ºC using a heat rate of 10 ºC/min under flowing air.

3.5.6. Raman spectroscopy

Raman spectroscopy was used to confirm the phase of TiO_2 as well as too know if any other molecules besides the expected titanium dioxide were present. Such is possible because different molecules and even different molecules polymorphs react differently to laser light, provoking distinct scattering phenomena. The samples were analysed using the TiO_2 particles suspended in water.

It was also used in films (all films except for C) to detect the presence of titanium dioxide. The Raman spectra were obtained a FT Raman spectrophotometer RFS 100/S (Bruker), with a 4 cm^{-1} resolution a YAG-Nd laser (1064 nm) as the excitation source and a He-Ne laser as the alignment source. Particles and films were scanned 500 and 2000 times, respectively.

3.5.7. Ultraviolet–visible spectroscopy (UV-Vis)

All films were subject to an UV- Vis spectroscopy to understand where each compound absorbs radiation and consequently to identify possible interactions between the added compounds in films T+P and TP. The UV spectra of the selected films were acquired between 250 and 850 nm, in a UV-Vis (Jasco V-560).

3.5.8. Fourier Transform Infrared spectroscopy (FTIR)

For the FTIR analysis of the films a Golden Gate single reflection diamond ATR reflection system (Perkin Elmer Spectrum BX) was used. The spectra were acquired at the absorbance mode between 4000 and 500 cm^{-1} (mid infrared region) with a resolution of 4 cm^{-1} and 32 scans per sample. Five replicates were collected for each sample.

3.5.8. Contact angle

The contact angles between ultra pure water and the films were determined using the system *OCA 20*, Dataphysics. The films were stored in a temperature-controlled chamber with Magnesium nitrate for humidity control. The films were cut into strips of 1x9 cm, 48 h before the beginning of the tests. The test used 3 µL of ultra pure water drops automatically dosed via syringe. The contact angles computations used *SCA20_M4*, Dataphysics software in the eclipse method. Each sample has 6 strips of film tested, and each strip has 10 drops of ultra pure water fall onto it.

3.6. Mechanical properties

The mechanical properties of the films were evaluated through tension until rupture tests following ASTM D 882 and 883 practices. The texturometer used was a TA-HDi, Stable Micro Systems. This method allows calculating deformation percentage, tension at rupture point and Young's modulus. The first lets us know the distance the film increases in its length from initial size until breaking due to the applied contrary forces (expressed in percentage), giving the information on elastic part of the films. The tension at rupture allows us to know what force needs to be applied to the films extremities, in opposite directions, to rupture. Young's modulus is a value used to express film elasticity, corresponding to the slope of stress-strain curves i.e it is achieved by dividing the tensile stress (MPa) by the extensional strain, in the elastic portion of the physical stress–strain curve (initial linear part). Tensile stress is the force applied which causes the film to stretch until immediately before its breaking point, causing film stretching. The extensional strain is a dimensionless value that expresses a proportion between the distance in the stretched film and its original length. It is found by dividing the difference in length before and after the film stretching (elastic phase) by its initial length.

The films were stored in a chamber with Magnesium nitrate to control its humidity and 48 h before the test the films were cut and market to the desired width and length (1 x 9 cm and 1x5 cm, respectively) and stored in the same chamber. The films were tested in a room with controlled temperature and humidity 60±5 and 26 ºC, respectively. The films thickness was measured immediately before the tests with a digital micrometer (*Digimatic Micrometer MDE-25PJ*, Mitutoyo). The tests were performed onto the 5 cm^2 of exposed film secured by the machine vertical grip system. The tests used a rate of 1.0 mm/s extensional deformation until sample rupture. Each sample had 6 strips to be tested.

3.7 Antioxidant activity

The antioxidant activity is determined with an adaptation of the acid 2,2'-azino-bis (3-ethilbenzotiazolina-6-sulfónico), ABTS method.

A solution of ABTS (Sigma-Aldrich) 7 mM in 2.45 mM potassium persulfate (Fluka) was prepared and left to react for 12-16 h in the dark at room temperature to form $ABTS^{+\bullet}$. From the $ABTS^{+\bullet}$ solution, 1 mL is diluted in 80 mL of ethanol (anhydrous, 99%, Carlo Erba) and its absorbance was measured at 734 nm in a *Jenway 6405* UV/Vis spectroscope. Its concentration is adjusted with ethanol in order to have an absorbance between 0.7 and 0.8. A square of 1 cm^2 of

film was put in 3 mL of the $ABTS^{+\bullet}$ solution and left to react in the dark for 7 days. The films antioxidant ability is measure with the following formula:

$$\%\ inibition = \left(\frac{abs_{control} - abs_{sample}}{abs_{control}}\right) \times 100$$

Where $abs_{control}$ is the value of absorbance of $ABTS^{+\bullet}$ solution (without film) and abs_{sample} is the value of absorbance of $ABTS^{+\bullet}$ solution with the film. Each sample has 3 replicas including the blank solution (the control).

3.8. Humidity

The determination of films humidity is accomplished by its drying until constant weight. Small aluminium foil shaped boxes are put in an oven at 105 ºC during 12-16 h. After cooling in a desiccator, the boxes were weighted. The film samples are cut into 4cm^2 squares placed in the tinfoil boxes and rigorously weighted. The films were placed in the oven at 105 ºC for a minimum of 16 h. After this time, they were placed to cool down in a desiccator for 30 min and then weighted. The film humidity is calculated with the following equation:

$$\%\ humidity = \left(\frac{m_{film\ i} - m_{film\ f}}{m_{film\ i}}\right) \times 100$$

Where $m_{film\ i}$ is the mass of the initial film and $m_{film\ f}$ is the mass of film after dried. The films humidity determination is made in triplicate.

3.9. Solubility test

The film solubility is determined in a matrix with water and sodium azide (0,02 % (w/v)) to inhibit microbiological growth. The solubility is determined through the films difference in mass before and after being immersed in water for a set period of time. A square of 4 cm^2 of film is first weighed and then put in 30 mL of a water and sodium azide solution and left at room temperature in an orbital shaker (80 rpm). The films were left in the water for 24 h and then put in a oven at 105 ºC for 16 h. The films were then cooled for 30 min in a desiccator and weighted. The films solubility is determined by the following equations:

$$m_{dried\ film\ i} = m_{film\ i} \times \left(1 - \left(\frac{\%humidity}{100}\right)\right)$$

$$Solubility = \left(\frac{m_{dried\ film\ i} - m_{dried\ film\ f}}{m_{dried\ film\ i}} \right) \times 100$$

Where $m_{film\ i}$ is the film initial mass, % humidity is the value determined with the procedure above, $m_{dried\ film\ i}$ is the initial mass of the dried film and $m_{dried\ film\ f}$ is the mass of film after it was submerged in the matrix and dried. All solubility determination trials were made in triplicate.

3.10. Statistical analyses

The results from the humidity, solubility, mechanical properties, contact angle and antioxidant activity were statically analysed using F-tests and t-student tests (Microsoft Exel 2010), to inquire if the samples were significantly different. The samples were considered significantly different when the significance level was $p \leq 0.05$.

Chapter 4 Synthesis and characterization of TiO_2 nanoparticles

4.1. Synthesis optimization

The TiO_2 particles were synthesized and characterised to be used as fillers in the biopolymer films. The objective was the preparation of monophasic homogeneous round-shaped particles of TiO_2 anatase. Several experiments were made with different temperatures (temperature series nr. 1 and 2) and times (time series) of reaction (see Table 3.1 at the Experimental Section). The samples of each series were analysed via SEM, X-ray, Raman spectroscopy, TEM, surface area, TGA-DTA to characterize particles. The first series of particles made was the "Temperature series nr. 1", in which temperature varies from 170 to 230 ºC for a time of reaction of 5 h.

Figure 4.1 shows the SEM micrograph images of the samples prepared at 170, 180, 190, 200, 215 and 230 ºC, over 5 of reaction. The selected conditions were chosen following the work reported by *Choi et al.* [64], describing the preparation of round-shaped particles with decreasing sizes when the reaction temperature increases from 110 to 150 and to 190 °C. From a first observation it is possible to conclude that all reaction temperatures lead to round-shaped particles with a textured surface. Moreover, the degree of aggregation of these particles varies with the temperature of synthesis. The sample 170_5h showed particles with a high variability of sizes. It seems that the round-shaped particles are connected by small nanoparticles. The sample processed at 180 °C presented more homogeneous particle size but the agglomeration of the particles was enhanced by the temperature. Further increase of the temperature to 190 °C leads even to higher degree of agglomeration. The particles at 200_5h maintained the round-shaped morphology and the agglomeration in this sample seems less evident. The aggregation apparently higher at 190 ºC than at 200 °C, may be explained by a continuous Ostwald ripening process in which smaller particles are dissolved to redeposit and form energetically favoured bigger particles. At 190_5h the process of dissolving can be at a high intensity while forming larger particles is still on its way, which contributes to the appearance of combined and not yet separated particles. The particles at 215_5h are mostly round-shaped but with smaller average size than the sample prepared at 200_5h. In this sample, the aggregation was slightly bigger than in 200_5h. The particles prepared at 230_5h (Figure 4.1) were almost completely aggregated. It can be observed that previously round-shaped particles were extremely aggregated which turned impossible to ascertain their size. This sample clearly does not present the desired properties.

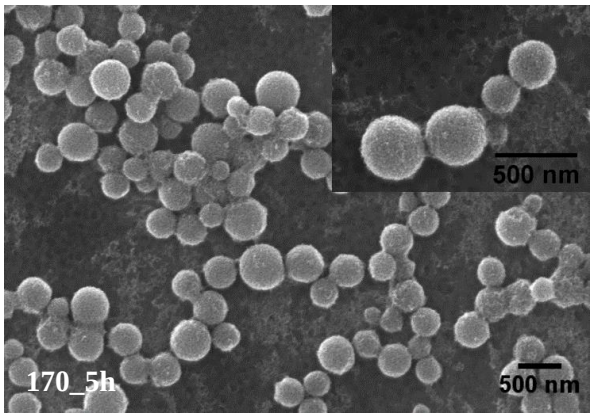

D_{SEM} = 415 ± 88 nm

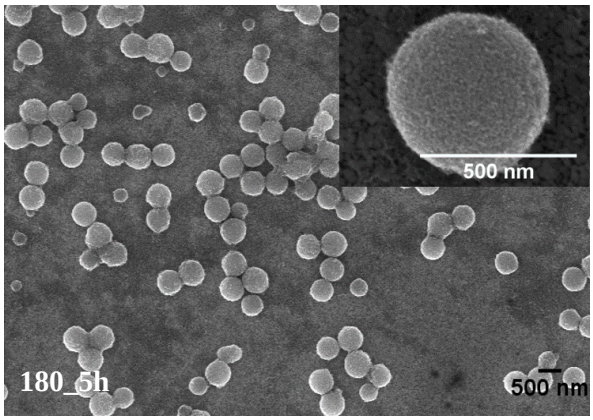

D_{SEM} = 481 ± 90 nm

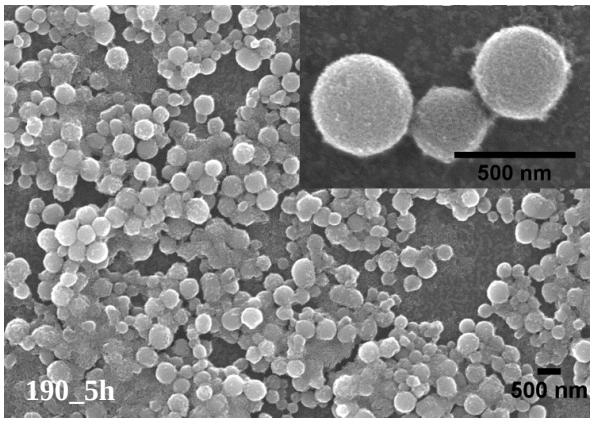

It is not possible to quantify particles size.

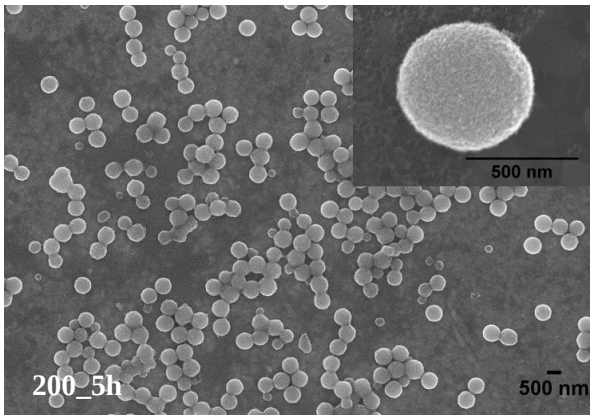

D_{SEM} = 554 ± 66 nm

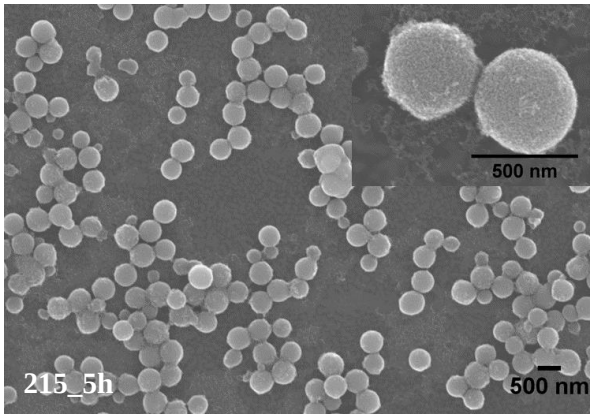

D_{SEM} = 392 ± 79 nm

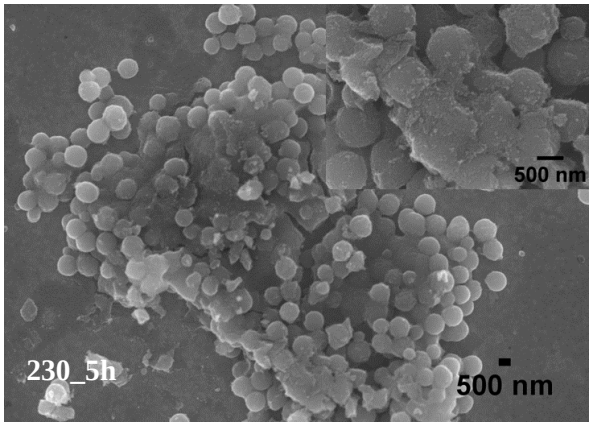

It is not possible to quantify particles size.

Figure 4.1- SEM micrographs of samples: 170_5h; 180_5h; 190_5h; 200_5h; 215_5h; 230_5h, indicating the average particle size obtained by measuring about 100 particles (D_{SEM}) using imageJ [88]. The insets show a higher magnified view of the particles.

With the analysis of this series temperature nr.1 SEM results, it became clear that 5 hours was an excessive amount of time for autoclaving the solutions. The sample with less aggregation is the

200_5h but even that sample appears to have too much aggregation. A new temperature series (temperature nr. 2) was made, reducing the reaction time from 5 to just 1 h.

The new series SEM micrograph images are displayed at Figure 4.2.

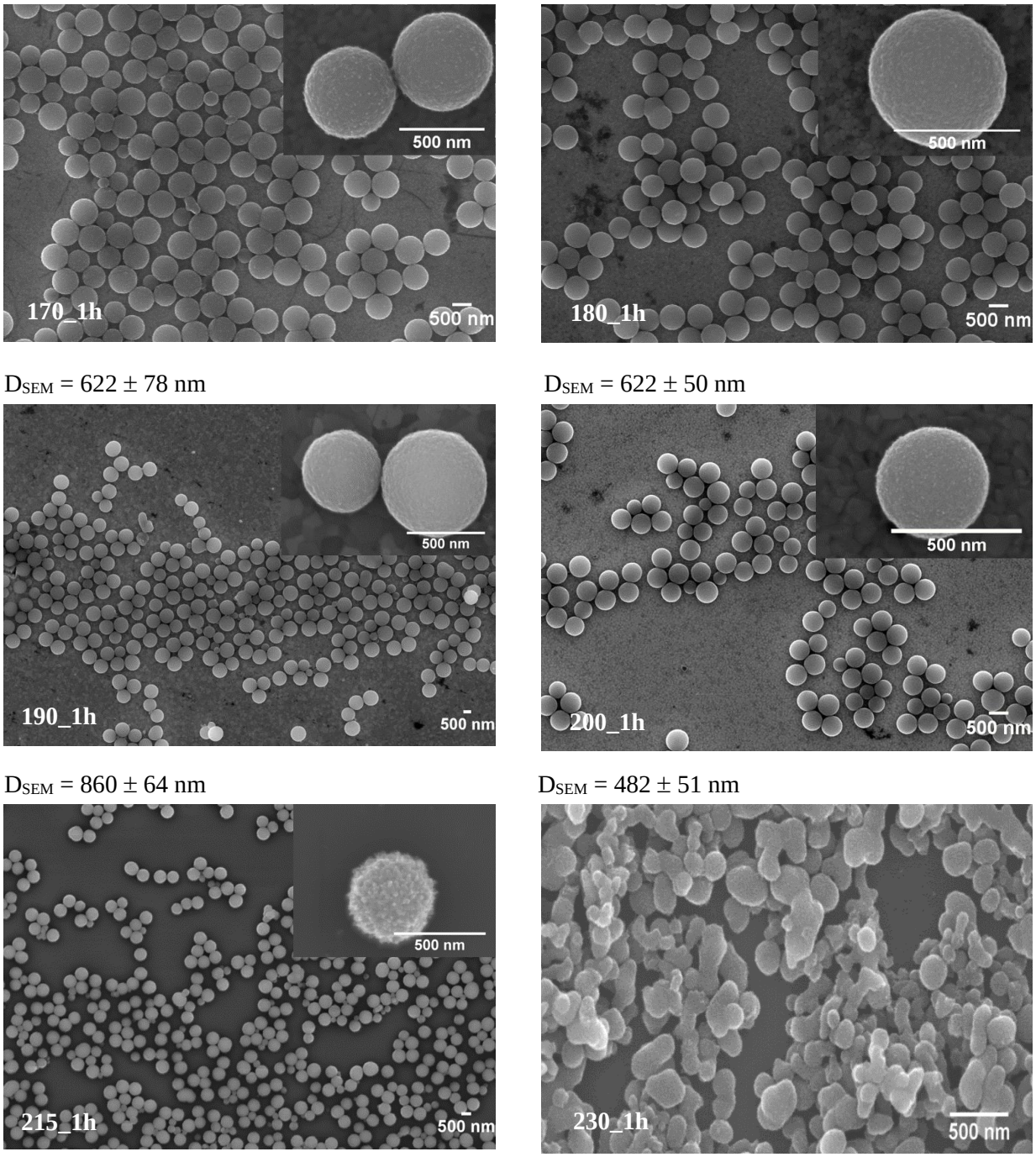

D_{SEM} = 622 ± 78 nm

D_{SEM} = 622 ± 50 nm

D_{SEM} = 860 ± 64 nm

D_{SEM} = 482 ± 51 nm

D_{SEM} = 571 ± 85 nm

Particles with anisotropic dendritic shape.

Figure 4.2- SEM micrograph images of series temperature nr. 2 of samples: 170_1h; 180_1h; 190_1h; 200_1h; 215_1h; and 230_1h. The average particle sizes obtained by measuring about 100 particles (D_{SEM}) using imageJ [88]. The insets show a higher magnified view of the particles.

The objective of SEM micrographs was to discover the effect of temperature in the size of the particles, expecting that they remain isolated. This was observed, with exception of sample 230_1h. This sample shows a kind of particle growth by aggregation of the round-shaped particles, to form a kind of dendritic structures. Apart from this sample, all the others prepared at lower temperature, show the round-shaped morphology with almost homogeneous sizes. A small noticeable detail, is that the sample at 215_1h (see inset) does appear to have more irregularities in its surface (i.e. it does not appear to be as smooth as the other samples). This however, appears to not interfere with other characteristics, since apart from the sample 230_1h, all the others (prepared at lower temperatures), show round-shaped morphology with almost homogeneous sizes and particles almost all isolated. As opposed to what was expected, the increase in temperature did not equate to a linear decrease in size (Figure 4.3).

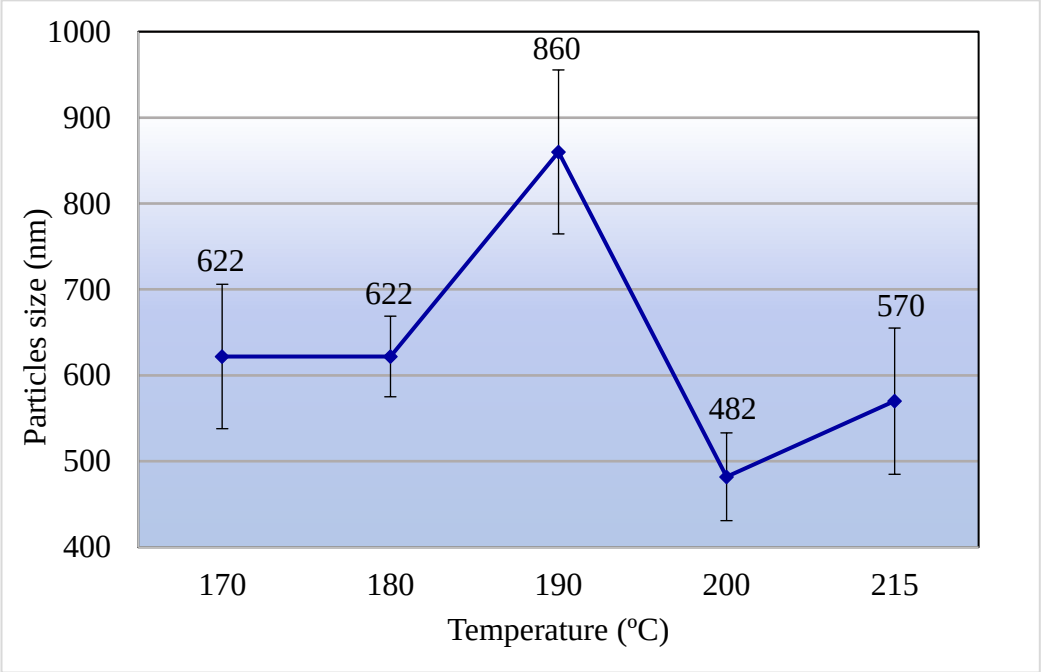

Figure 4.3 . Particles size distributions of temperature series nr. 2 (1h).

This series (temperature nr. 2) was also analysed by X-Ray Diffraction (XRD) since it is important to know crystallographic phase of TiO_2, in the different samples one of the criteria was to ultimately have particles made of only one crystallographic phase of TiO_2 (Figure 4.4).

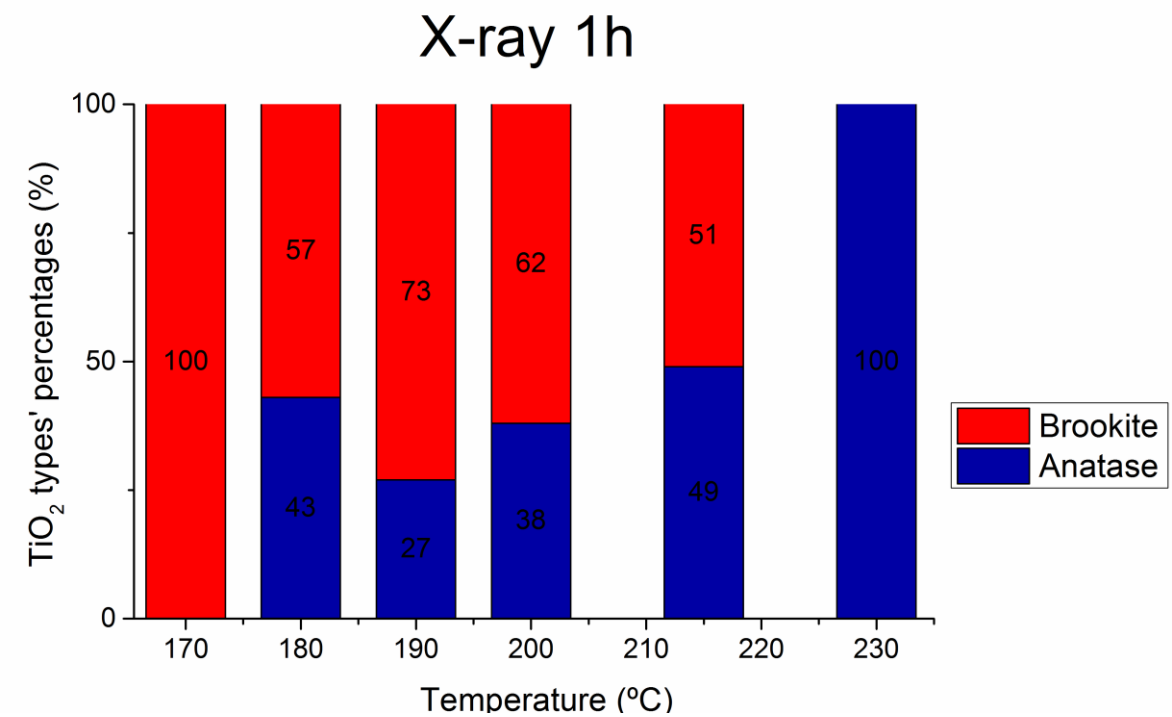

Figure 4.4. Crystallographic phase content (in percentage) in series temperature nr. 2 as determined by XRD data analysis.

From the analysis of the results only the samples 170_1h and 230_1h present one crystallographic phase. The sample prepared at the lowest temperature was formed by 100% of brookite, while the sample processed at 230 °C was constituted by pure anatase. At the intermediate temperatures, it was observed the successive decrease of brookite with consequent increase of anatase phase. The tendency is that the amount of anatase increases with the increase in temperature, except for the sample at 180 ºC that has more anatase than expected. It is believed that this last result is a bit away from the trend due to any experimental variability.

The sample 230_1h has the desired condition of only one type of TiO_2. However, as seen in SEM images (Figure 4.2), this sample lacks shape uniformity. So, it became clear that a time refinement of one of these temperatures would have to be made. After analysing the SEM micrographs of this series, the temperature of 200 degrees was chosen as the one for which time should be adjusted. Thus, the series denoted "time series" was prepared maintaining the 200 °C temperature constant and varying the time of synthesis from 1 to 5 h. The objective of this series (which SEM micrographs are displayed in Figure 4.5) was to further reduce particle size while avoiding aggregation and to obtain monophasic particles of pure anatase.

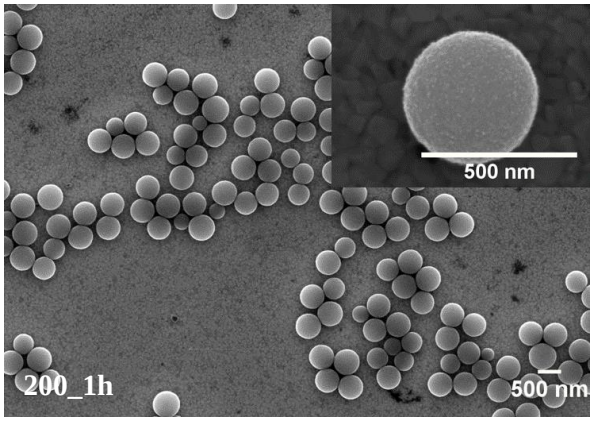

D_{SEM} = 483 ± 51 nm

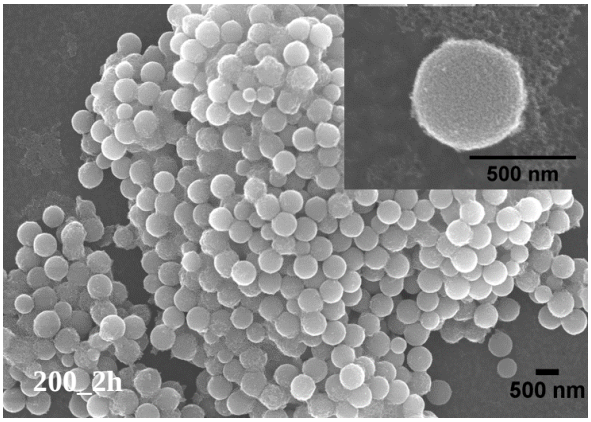

D_{SEM} = 480 ± 62 nm

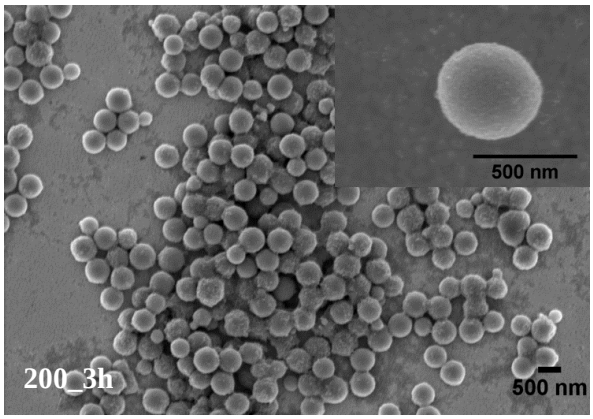

D_{SEM} = 457 ± 112 nm

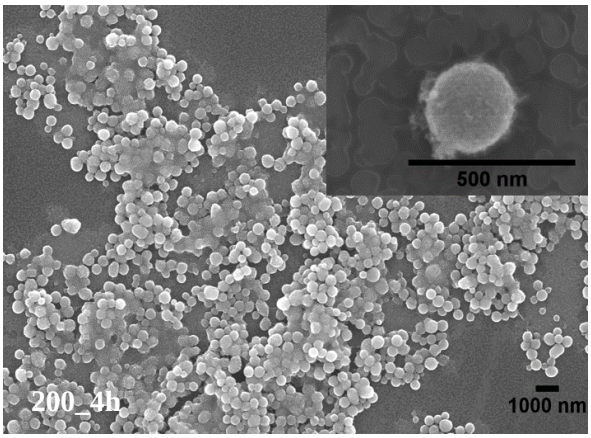

It is not possible to quantify particles size

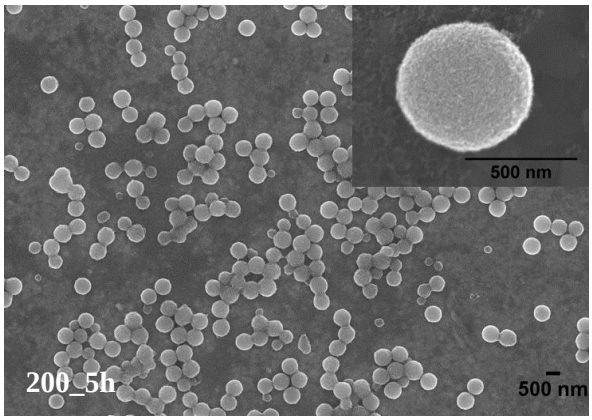

D_{SEM} = 554 ± 66 nm

Figure 4.5 SEM micrograph images of TiO_2 particles synthesized during various times of hydrothermal synthesis: 200_1h; 200_2h; 200_3h; 200_4h; and 200_5h, showing average particle size (D_{SEM}) measured using about 100 particles using imageJ [88]. The insets show a higher magnified view of the particles.

The sample 200_1h presented good characteristics in both shape and size but was mainly formed by brookite. The samples at 200_2h and 200_3h also presented good results in size and shape of particles even if aggregation was starting to increase. The sample 200_4h was too aggregated to be considered for further use. The sample at 5 hours, as it was not so aggregated,

was also tested in X-ray along with the aforementioned samples. Figure 4.6 shows the hourly progression of TiO_2 anatase percentage formation at 200 °C.

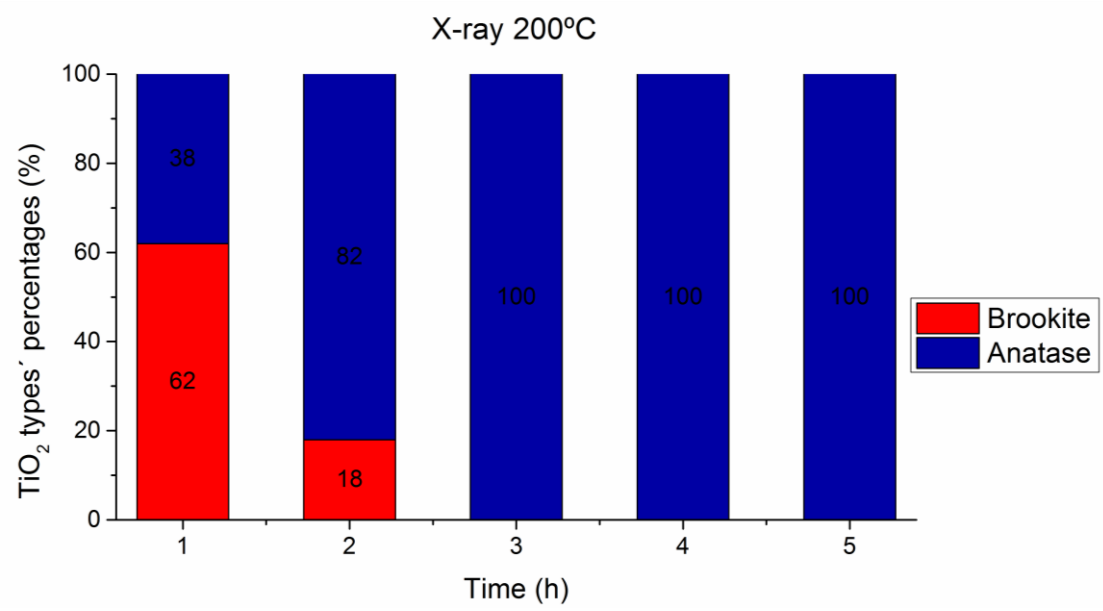

Figure 4.6. Crystallographic phase content (in percentage) in series time determined by XRD data analysis. Above 3 hours of reaction under the specified conditions, it is always achieved anatase pure phase.

According to the XRD results, samples 200_1h and 200_2h presented two crystallographic phases of TiO_2 (anatase and brookite) while the sample at 200_3h, 200_4h and 200_5 h only had anatase. Since the preferable outcome was to have only one type of titanium dioxide in the particles, the 3 h and 5 h sample became the front runners for latter incorporation in the chitosan films. The sample at 3 h has problems with aggregation and the sample at 5 h has an average particle size above 500 nm. Since the sample at 3 h presented small particle size, a new sample was prepared with 2.5 h of hydrothermal treatment. The idea was to maintain the size below 500 nm while reducing the aggregation degree.

This new sample (200_2.5h) was analysed by SEM as shown in (Figure 4.7) and by XRD analysis (Figure 4.8). This sample shows a slight decrease in aggregation and the particles were only formed by anatase.

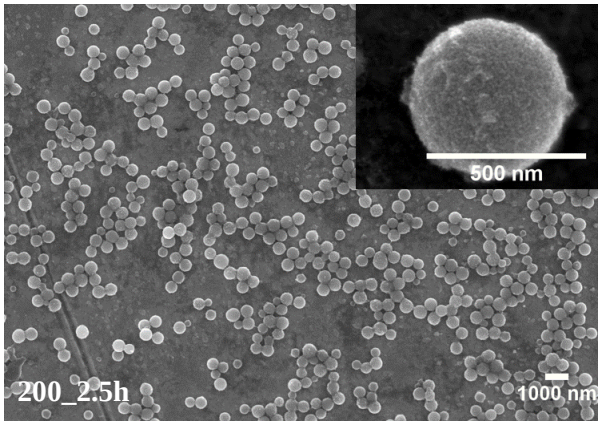

D_{SEM} = 437 ± 67 nm

Figure 4.7 - SEM micrograph of TiO_2 sample synthesized during 2.5 h at 200 ºC (200_2.5h) of hydrothermal synthesis.

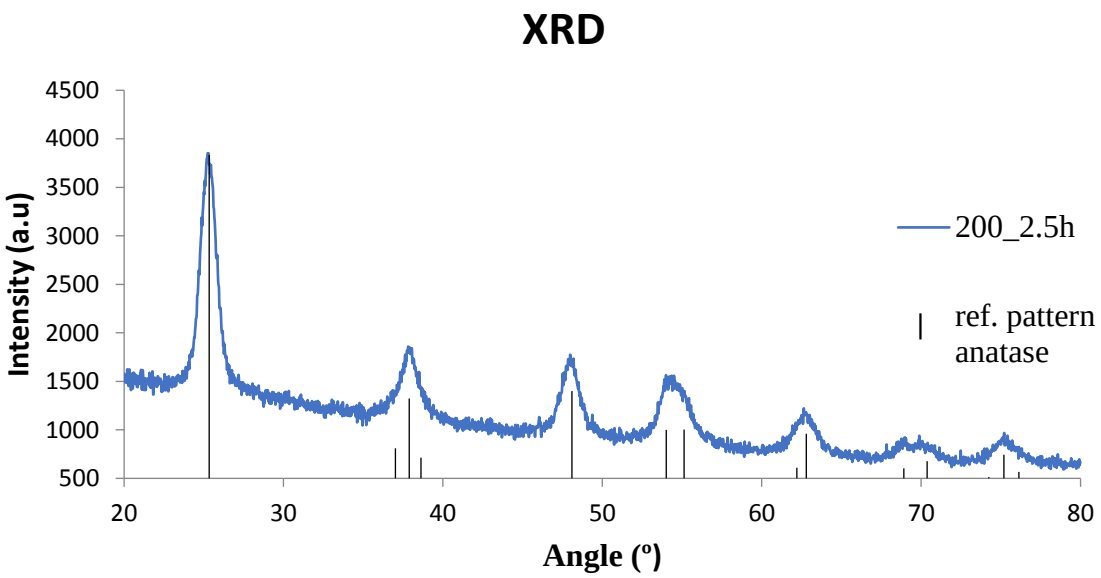

Figure 4.8 – XRD analysis of 200_2.5h against reference pattern anatase (nr. 04-016-2837).

4.2. Characterization of the selected samples

The crystallite size was calculated from the Scherrer equation for samples at 200 ºC for 1, 2.5, and 5 h and the calculated particles sizes varied from 4 to 9 nm when reaction time increases from 1 to 5 hours, which is a much smaller than the size determined by SEM analysis.

In order to better understand the morphology of the samples, the samples 200_1h, 200_2.5h, and 200_5h, were analysed by TEM (Figure 4.9). The first evidence is that the particles previously

observed in SEM (Figure 4.1, Figure 4.2, Figure 4.5 and Figure 4.7) were made of smaller TiO_2 crystallites, compatible with the size determined on the XRD (4-9 nm).

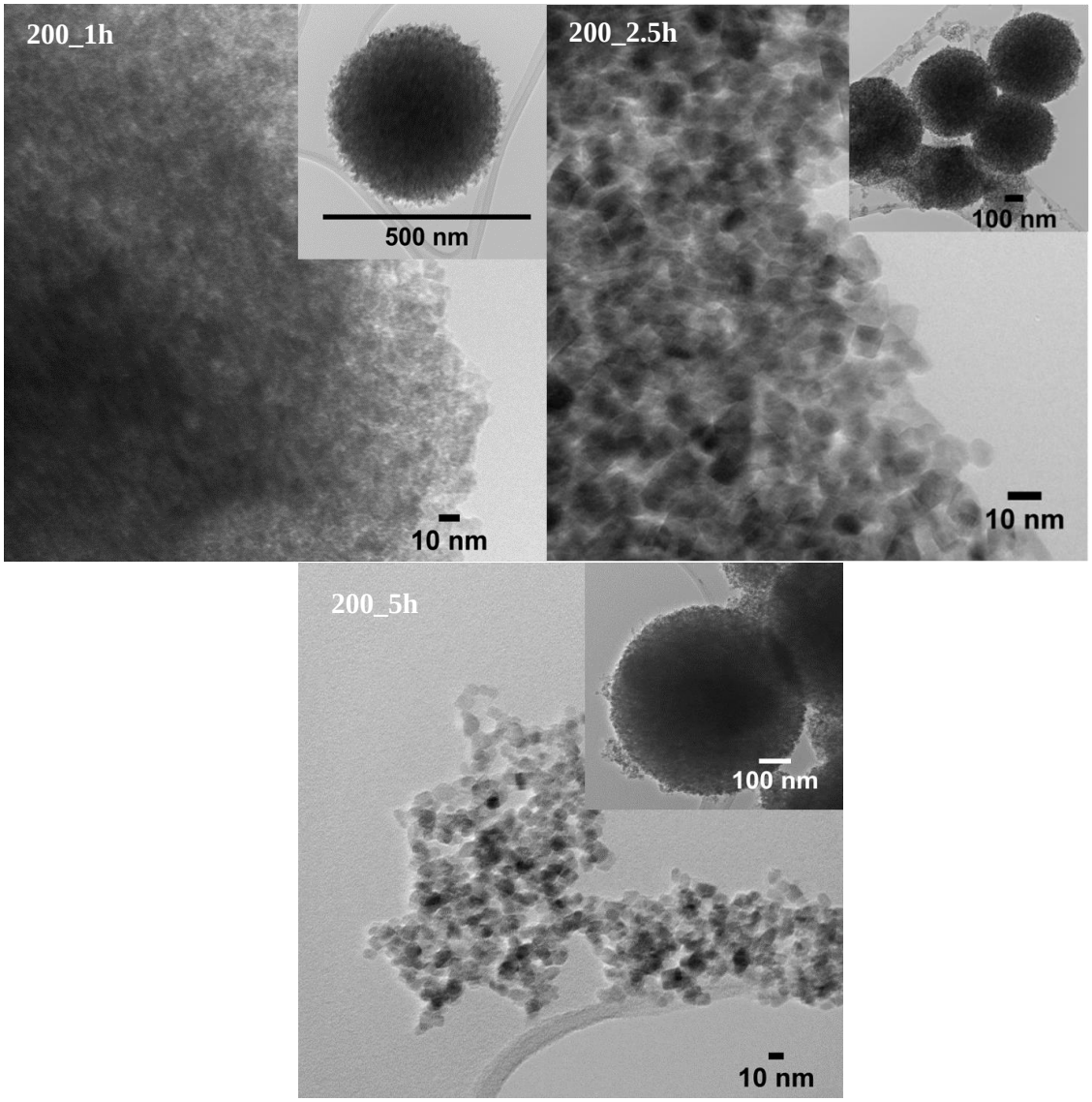

Figure 4.9 TEM micrographs of TiO_2 particles synthesized at 200 °C during various times of hydrothermal synthesis (1, 2.5 and 5 h), illustrating that the round-shape particles were formed by very small crystallites.

In the sample prepared in just 1 h (Figure 4.9) the crystallites are not very well formed, indicating an amorphous character. After 2.5 and 5 hours of reaction, the crystallites are better crystallized as evidenced by the strong contrast. These crystallites are very aggregated and have general sizes below 10 nm (Table 4.1).

The TEM image of the sample 200_1h (Figure 4.9) shows very small crystallites with a non-defined shape and low image contrast, indicating pseudo-crystallized character typical of the

brookite phase. Oppositely, the samples after 2.5 and 5 hours of reaction display well-crystallized crystallites, as evidenced by the strong contrast and facetted crystallites. These results are in agreement with the XRD analyses, which indicate in both samples the presence of anatase. Moreover, the crystallites are very aggregated to form the round-shaped particles (clearly visualized in the SEM and TEM) and have general sizes below 10 nm (Table 4.1). The crystallites of 200_1h cannot be measured via TEM because of their lack of defined edges and small size. Again, these TEM results are compatible with the values determined using the Scherrer equation (see Table 4.1).

Table 4.1 – Average crystallite sizes obtained via X-ray, average crystal sizes observed in TEM (D_{TEM}), SEM (D_{SEM}) and specific surface area (A_{BET}) of samples prepared during 1, 2.5 and 5 h of hydrothermal synthesis.

Sample	D_{XRD} (nm)	D_{TEM} (nm)*	D_{SEM} (nm)*	A_{BET} (m^2/g)
200_1h	3.71	-	483 ± 51	234 m^2/g
200_2.5h	7.85	8 ± 2	437 ± 67	162 m^2/g
200_5h	8.85	9 ± 1	554 ± 66	98 m^2/g

*Measured with imageJ.

To further investigate the structure of the obtained samples, Raman spectroscopy measurements were performed. Figure 4.10 shows the Raman spectra of samples 200_1h, 200_2.5h and 200_5h. The Raman spectrum of the sample 200_1h is formed by an intense band at 149 cm^{-1} and several weak bands at 322, 404, 448, 453, 515 and 633 cm^{-1} (Figure 4.10 -black). According to literature, brookite Raman spectrum is characterized by strong band at 153 cm^{-1} and a medium intensity band at 636 cm^{-1} [90]. Weaker bands at higher wavenumbers are also expected. Brookite spectrum is not as simple as anatase and rutile spectra due to its reduced crystal symmetry [90].
The samples 200_2.5 h and 200_5h possess different Raman patterns very similar to the reported pattern of anatase, having a very intense sharp band at 144 cm^{-1} (E_g), four bands at 197 (E_g), 399 (B_{1g}), 516 (A_{1g}, B_{1g}) and 639 (E_g) cm^{-1} as well as three weak combinations bands near 796 (B_{1g} overtone), 695 (combination) and 320 cm^{-1} (combination) [91, 92]. This observation corroborates the XRD results, indicating that both samples (200_2.5 h and 200_5h) are constituted mainly by crystalline anatase. A nearly identical spectrum was achieved by Warwick et al. [92] with the hydrothermal production of TiO_2 using titanium(IV) bis(ammonium lactato)dihydroxide as metallic precursor.

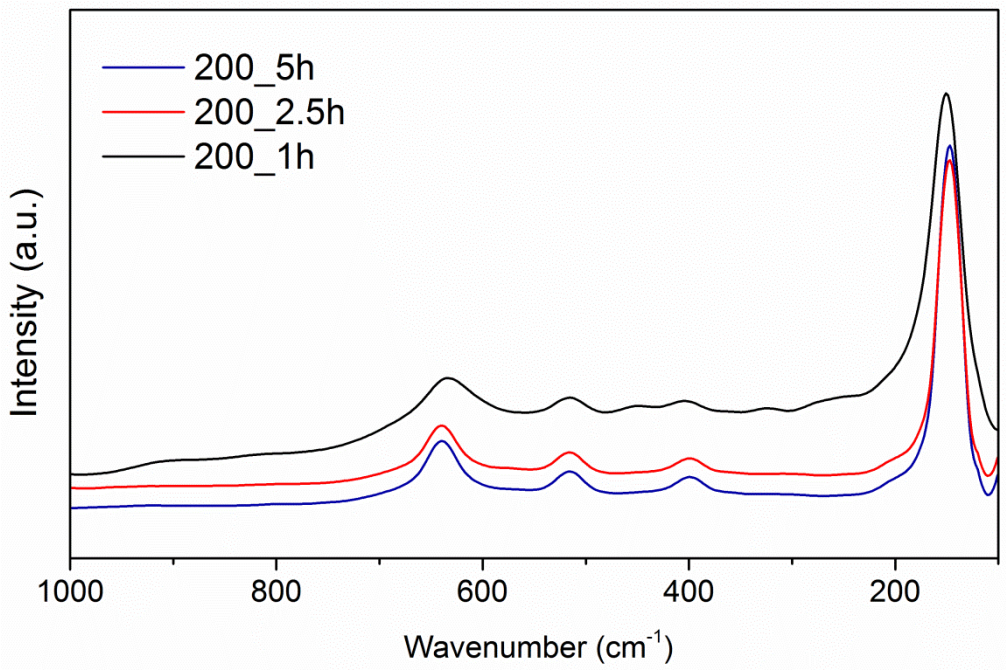

Figure 4.10 – Raman spectrum of 200_1h, 200_2.5h, and 200_5h samples.

The samples appear to have a decreasing specific surface area (A_{BET}) with the increase of time of synthesis (Table 4.1**).** The decrease of A_{BET} is inversely proportional to the increase of particle size observed by TEM. From these results, it could be said that crystallites at 1 h are smaller than the ones prepared over 2.5 and 5 h, possessing a larger specific surface area. Considering also that the crystallites are aggregated forming the round-shaped particles observed by SEM (Figure 4.5 and Figure 4.7), it is possible to generalise that the assembly of the crystallites increases with time, decreasing its distance from each other, which decreases the available specific surface area.

Thermal gravimetric (TGA) analysis were made to know if compounds were adsorbed in the particles surface, and if so at what temperature did they decompose and leave the particle decreasing its weight. The differential thermal analysis (DTA) can help identify possible reactions that occur with temperature increase.

The TGA curve (black line) shows the weight loss during heating. The biggest weight loss of the 200_1h sample (14.3%) occurs up to 285 ºC (region I - Figure 4.11) and can be attributed to water loss, hydroxyl groups and decomposition of organic components such as acetonitrile and ethanol. According to literature acetonitrile decomposition temperature is over 120 ºC [93] and ethanol is above 200 ºC [94]. In region II, the sample continues to lose weight but at a lesser extent, the loss can be attributed to organic compounds such as methylamine (decomposition temperature above 550 ºC) [95] among others. Above 400 ºC no other remarkable weight loss was observed.

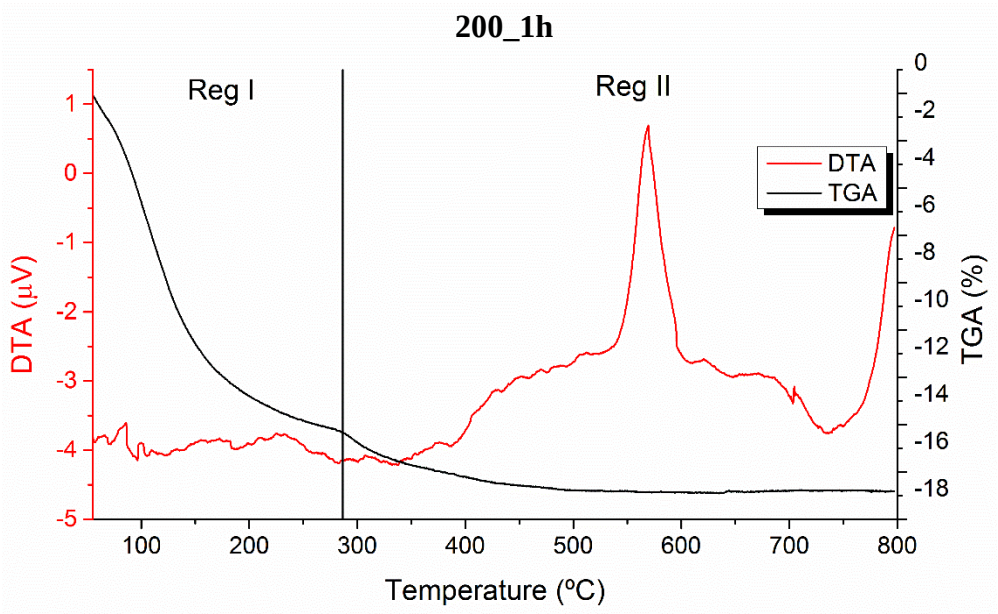

Figure 4.11. Differential thermal (DTA) and thermal gravimetric (TGA) analysis of 200_lh sample illustrating the loss of the adsorbed water, hydroxyl groups and decomposition of organic compound residues. It is observed the thermal formation of anatase phase at 570 ºC.

Regarding the DTA curve (red line) a peak at 570 ºC could indicate an exothermal transformation of brookite into anatase. This explanation is supported by the absence of similar peaks on the DTA analyses of samples 200_2.5h (Figure 4.12) and 200_5h (Figure 4.13), which were already formed by anatase. The transformation into rutile is considered not plausible as it would be expectable the transformation of brookite into rutile below 600 °C.

200_2.5h

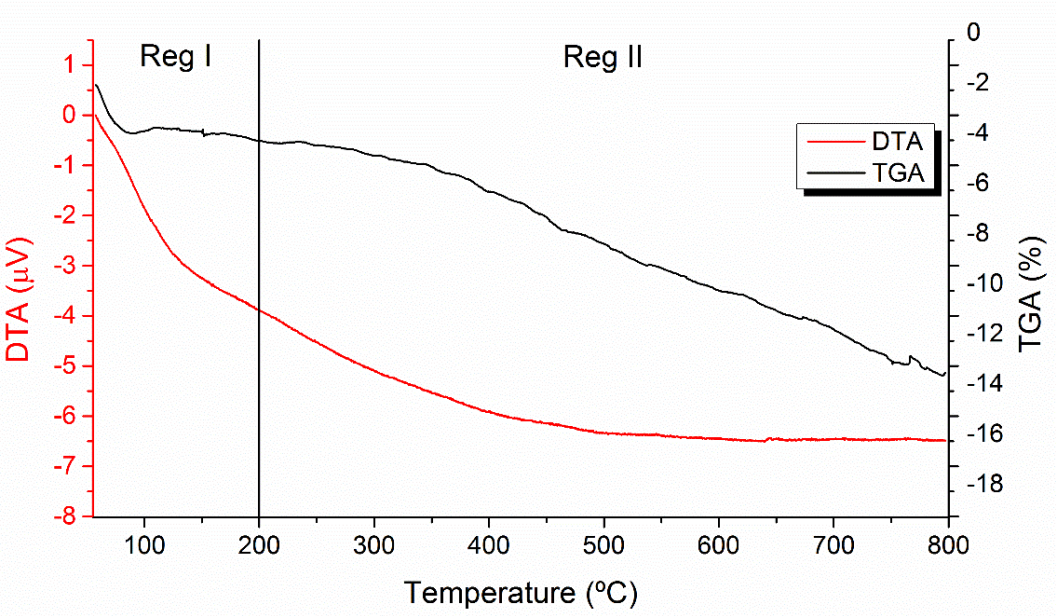

Figure 4.12 – Differential thermal (DTA) and thermal gravimetric (TGA) analysis of 200_2.5h sample, illustrating loss of adsorbed water, hydroxyl groups and organics decomposition.

The sample at 2.5 h also suffered from a weight loss of 12.3% of its initial weight. This loss is gradual, having a greater weight loss around 100 ºC attributed to water [96]. In region II (Figure 4.12) the weight loss is attributed to the desorption of hydroxyl groups on the particles surface and combustion of organic compounds [97]. The DTA curve in red shows no peaks. From the results, it appears neither significant exo- nor endo-thermal reactions occur, indicating the maintenance of the anatase phase till 800 °C.

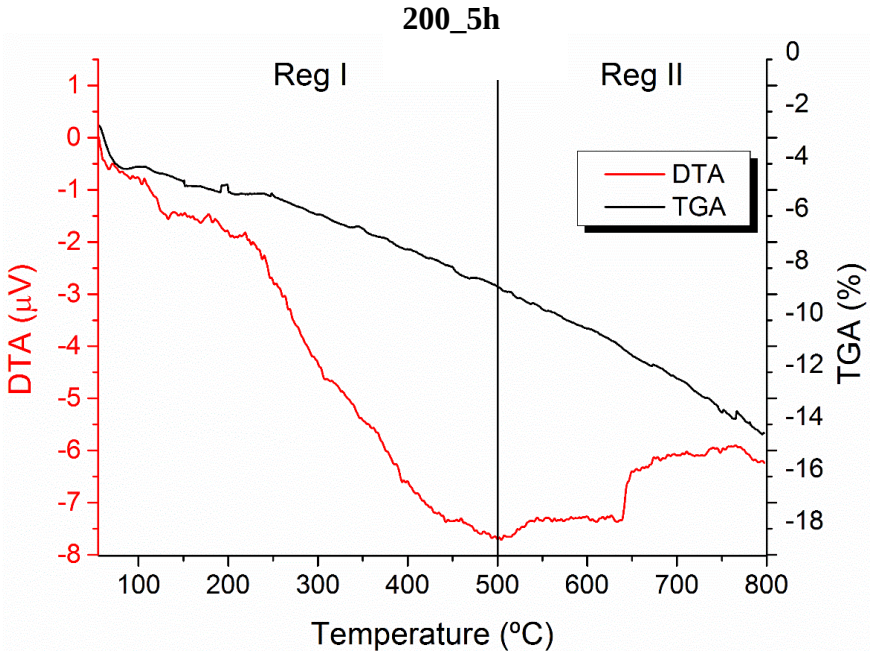

Figure 4.13 - Differential thermal (DTA) and thermal gravimetric (TGA) analysis of 200_5h, illustrating loss of adsorbed water, release of hydroxyl groups and decomposition of organic compounds.

The sample at 5 h suffers a weight loss of about 13.3% (Figure 4.13) of its initial weight. It has a TGA curve similar to sample 200_2.5h, including the water loss around 100 ºC and weight loss attributed to organic compounds and hydroxyl groups from the particles surface.In region II, at around 645 ºC (red line), it can be observed an area with peaks denoting an exothermic reaction. This usually means that crystallization occurred. As the X-ray diffraction of the 200_5h sample indicated that this sample was formed by 100% anatase, this exothermal peak could indicate a phase transformation from anatase to rutile, which is typically expected at around 600 ºC. This peak is not present in 200_2.5h sample potentially because this sample was exposed to elevated temperature and pressure for a smaller amount of time (2.5 h versus 5 h). So, it absorbed less energy and it is kinetically behind on energy, which could explain the lack of phase transition.

After analysing all the above results the sample 200_2.5 h was selected for the further incorporation as filler on the biopolymer films due to its size (< 500 nm), round size, anatase polymorph of TiO_2 and low aggregation amount.

The importance of methylamine

Pararelly to the search for the ideal conditions for the desired TiO_2 particles, additional work was done in order to understand the role of methylamine (a primary amine) and to determine if it could be substituted for ethylamine (a tertiary amine). The idea to further investigate the primary amine came about because, the amounts used in the synthesis were so small (6.9 µL), one wondered how impactful they truly were in the particles formation process. As a result, an amine series was made.

Several iterations of the same protocol were made with two distinct amines and with different amount of the amine used in the particles normal synthesis (methylamine) (see Table 3.2 at the Experimental Section). The set conditions for temperature and time were 200ºC and 5h, respectively because it was thought that since this sample had what was considered a midland amount of aggregation, it would be possible to assess if the aggregation increased or decreased.

SEM (Figure 4.14) was used to visualize the impact of the different conditions experimented upon, on the particles morphology and aggregation.

By observing the SEM result of 200_5h_none (Figure 4.14) it can be inferred that methylamine does need to be used since its absence results in very few, dissimilar looking, particles, both in shape and size.

The amount used (6.9 µL) in the protocol appears to be the ideal, since increased amounts (200_5h_3XM) it did not allow the formation of spherical particles. For the sample 200_5h_E we observed that methylamine can in fact be substituted for another amine in this case ethylamine, a tertiary amine. Ethylamine could provide the needed steric and electrostatic stabilization at the same levels as methylamine, resulting in spherical TiO_2 particles.

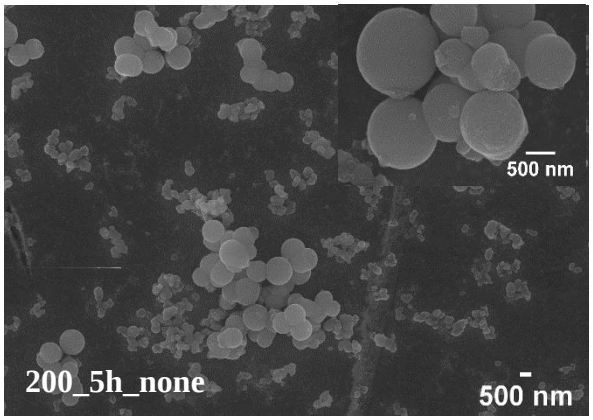

It isn't possible to quantify particles size.

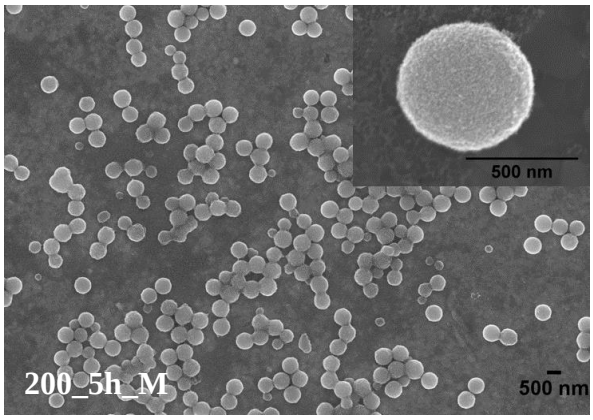

D_{SEM} = 554 ± 66 nm

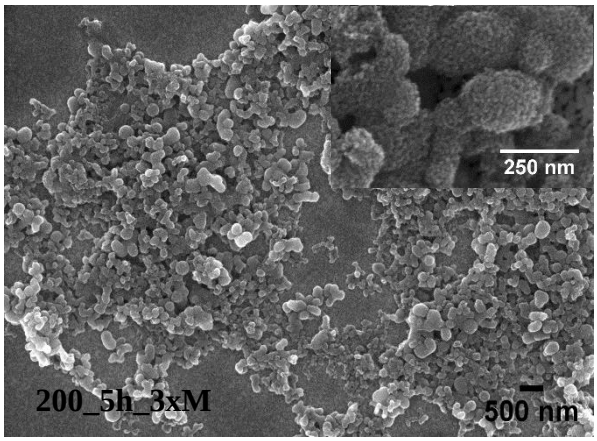

Heterogeneous and extremely aggregated

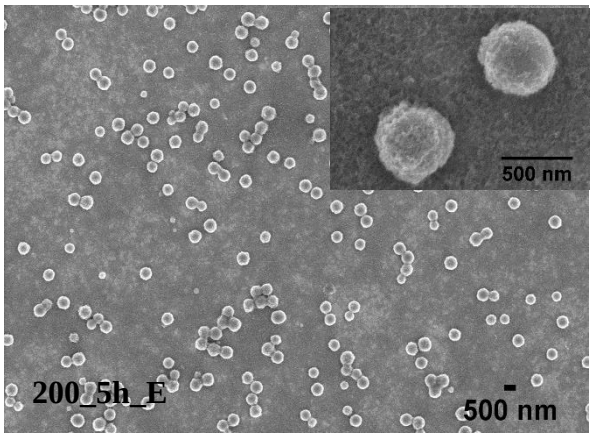

D_{SE} = 457 ± 70 nm

Figure 4.14- SEM micrographs of samples: 200_5h_none; 200_5h_M; 200_5h_3xM; 200_5h_E, indicating the average particle size obtained by measuring about 100 particles (D_{SEM}) using imageJ [88]. The insets show a higher magnified view of the particles.

Chapter 5 Synthesis and characterization of chitosan films

In this chapter, the 5 films that were made (protocol in 3.1 in experimental section) were put through a series of test so that the best option for packaging could be found. Figure 5.1 shows the films prepared in this work films: C (just chitosan), T (chitosan and TiO_2), P (chitosan and phenolic compounds), TP (chitosan, TiO_2 and phenolic compounds added simultaneously) and lastly T+P (chitosan, TiO_2 and Phenolic compounds added at different times).

The TiO_2 was chosen expecting a betterment in the films barrier properties, the gain of an oxygen scavenger ability, biocide capacity upon under UV-radiation and sensor possibilities. Phenolic compounds extract was used expecting the entrust in films increased antioxidant ability and sensor capacity (mainly in colourimetric methods).

Each film has about 0.47 g of chitosan and have about 9.3 mg and 4.1 mg of nanoparticles and phenolic compounds/pigment, respectively, depending on the components used.

Observing Figure 5.1 one can see that film C does not have any colour and is transparent. Film T is white and has some opaqueness (provided by the TiO_2 particles). Film P is transparent with a very light green tint (provided by the phenolic compounds). The films TP and T+P have some opaqueness provided by the TiO_2 particles but then they differ in colour. The film TP is believed to have more interaction between the particles and the pigment resulting in a green colour. The film T+P seems to not have that same interaction, resembling the colour of the pigment extract (Figure 5.2).

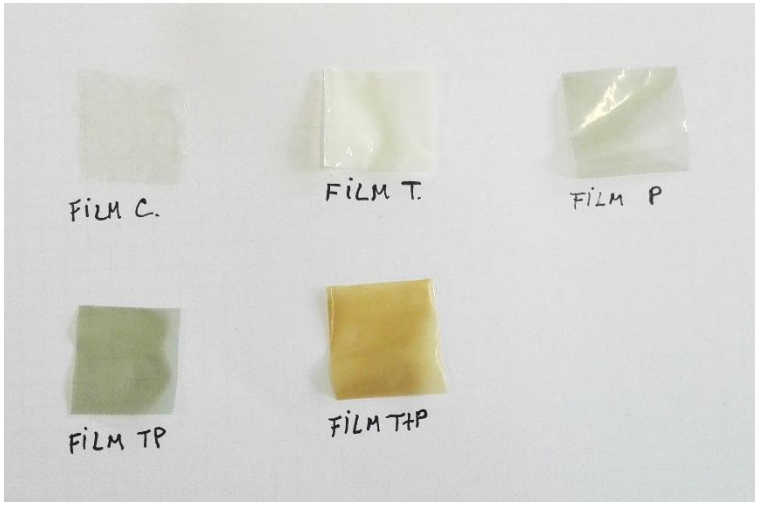

Figure 5.1 – Photo of squares of 4 cm^2 of the films. The films designations follow Table 3.3 from the experimental section.

The film preparation was optimized regarding the amount of glycerol and nanoparticles used. Initially 50% of glycerol (w/w) in relation to chitosan was used but the films became too sticky an

undesired characteristic, so decreasing amounts of glycerol were tested. The best films, evaluated just by handling the film and manually stretching, were obtained using 25% glycerol (w/w).

The amount of particles used was also tested in 3 batches with 2, 5 and 10% (of the amount of chitosan used (w/w)). The resulting films were observed for opacity (undesired) and for particles ability to disperse in the films matrix. All films had, at the naked eye, good dispersion, however films at 5 and 10% were too opaque for the desired appearance. Therefore, 2% of particles were used for further characterization of the films.

The extract obtained from black rice was quantified for its phenolic compounds using the Folin-Ciocalteau method. Figure 5.2 shows the pigment (approximately 45.32 mg that is about 0.15 ± 0.03 % (w/w) of dried powder black rice), after concentration, to be used in the films production.

Figure 5.2 - Phenolic compounds/pigment after concentration of about 45.32 mg of phenolic compounds.

5.1. SEM

All prepared films were morphological characterised using SEM. Both top and transversal views were analysed in order to verify the homogeneity of the films and the particles dispersion within the bionanocomposite. Figure 5.3 display the micrographs of all 5 films.

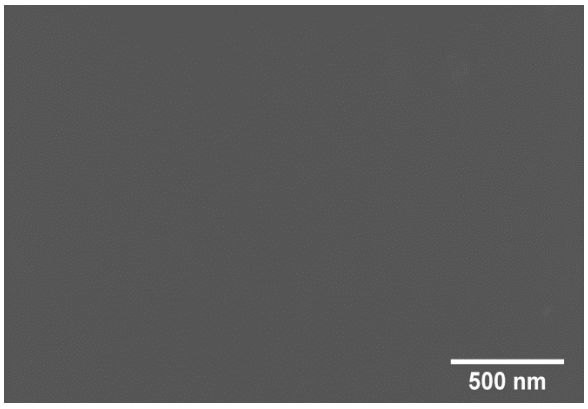

Film C top view

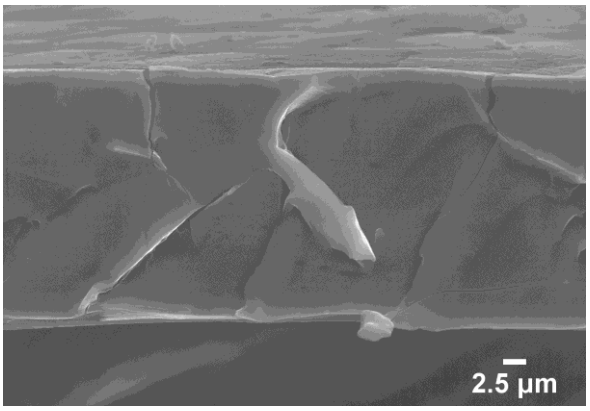

Film C transversal view

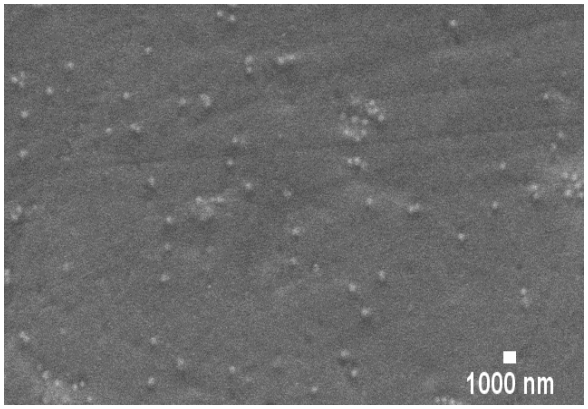

Film T top view

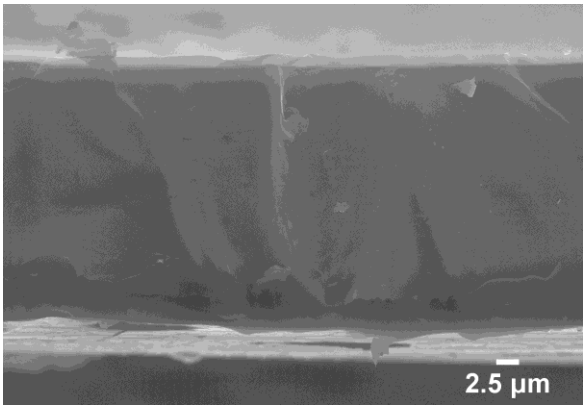

Film T transversal view.

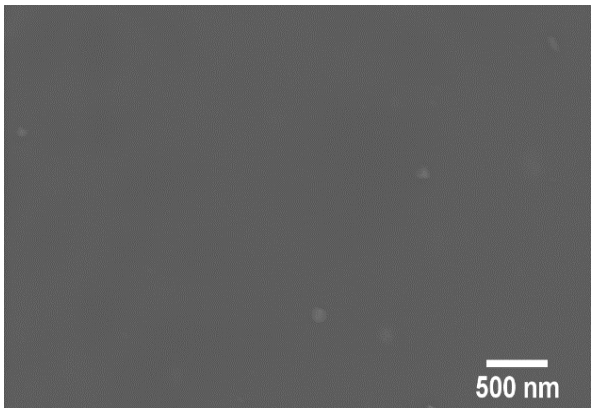

Film P top view

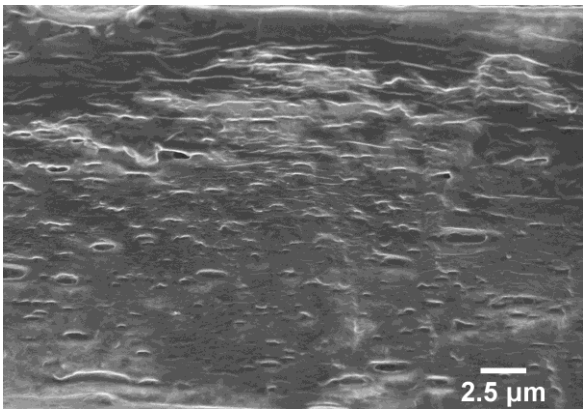

Film P transversal view

Figure 5.3– SEM micrographs of films C, T and P, from surface and transversal views of the films.

From the micrograph in Figure 5.3 it can be observed that film C is homogeneous and does not have any detectable defects. In the film T, the TiO_2 particles can be observed in the film and appear to be well dispersed in the films surface. The particles are not evident in the films cross-section view. Film P just like film C appears to be very homogeneous. However, its transversal or cross-

section view, displays a heterogeneous matrix probably due to the interaction between pigment and chitosan.

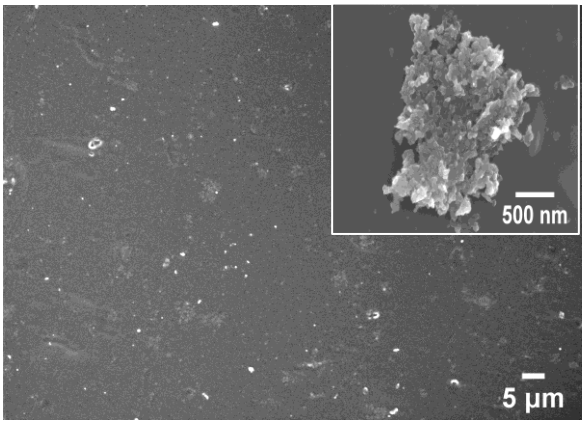

Film T+P above view

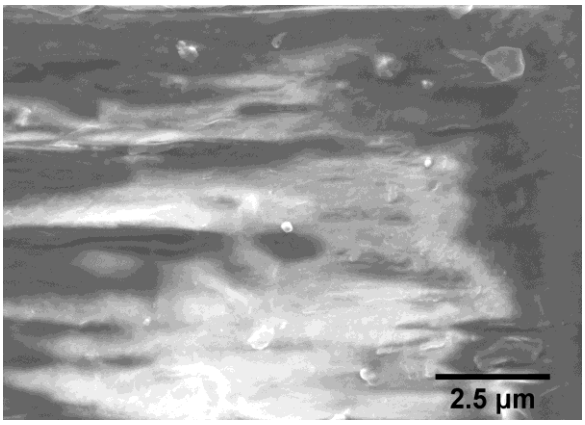

Film T+P transversal view

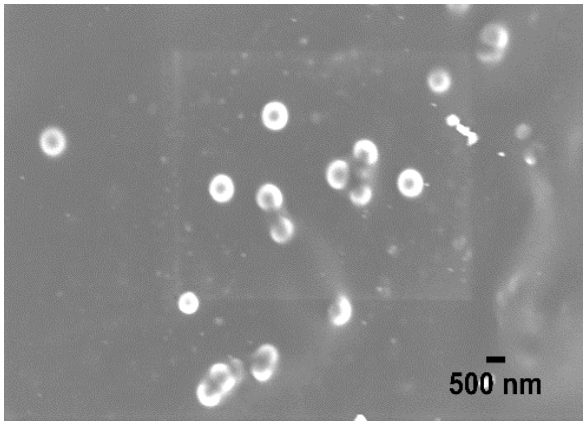

Film TP above view

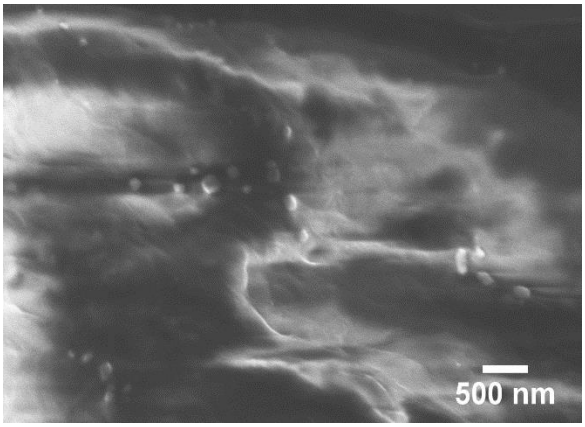

Film TP transversal view

Figure 5.4– SEM micrographs films, T+P and TP. The micrographs were taken from the surface and transversal view of the films. Under the micrograph it is specified which film and view type it is.

Film T+P (Figure 5.4) has well dispersed particles like observed in film T. However, observing the inset it is possible to infer that the nanoparticles seem to, at some point, have desegregated to a degree, that caused them lose the round-shaped form observed in the SEM micrograph of the pure TiO_2 prepared at 200 °C over 2.5 h. The cross-section view shows a similar trend with the one observed for film P. In the case of the film TP, the nanoparticles seem to remain aggregated into round-shaped particles with less than 500 nm. These particles are dispersed within the chitosan matrix.

5.2. UV-Vis

UV-Vis spectroscopy was used to better understand how the compounds added alter the way the chitosan films absorbs light and to know if there are bands in the areas typical of the added compounds, as well as to observe any shifts indicating possible interactions between compounds. Figure 5.5 shows the UV-Vis spectrum of all 5 films.

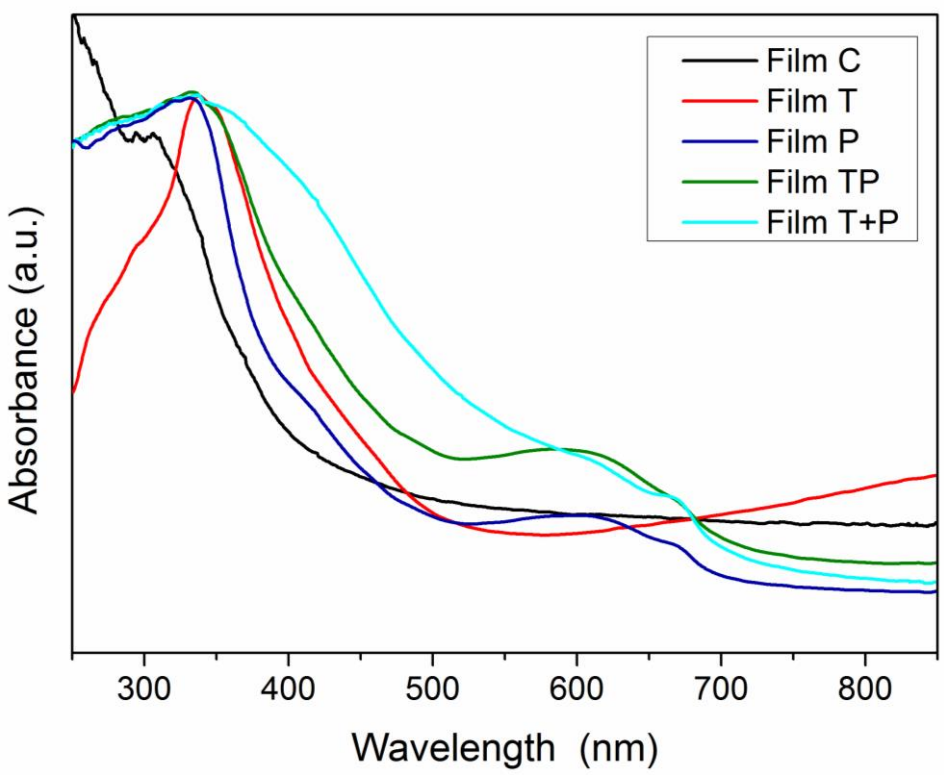

Figure 5.5– UV-visible light spectra of all films (C, T, P, TP and T+P).

All films have a peak at around 330 nm, and since all they have in common is chitosan, that peak is attributed to this biopolymer. Chitosan has no peaks in the visible range supporting its transparency.

Film T has also a peak at a slightly higher wavelength, which is attributed to the titanium dioxide. Commercially available anatase titanium dioxide has peaks at around 350 nm, supporting this observation. [98].

Film P has the aforementioned chitosan attributed peak, at 330 nm, but it also has a large band from 250 to about 350 of phenolic compounds [99] as well as a shoulder at around 600 nm that can also be attributed to phenolic compound (mainly anthocyanins), this is also supported by literature [100].

Films TP and T+P are similar although the phenolic compound shoulder (aprox. 600 nm) is not as defined in T+P. An explanation could reside in the fact that the T+P film has a yellowish colour while the TP film has a green tint; and since yellow absorbs light at around 450 nm versus 650 nm in green [101], the contribution of the yellow to the phenolic compound shoulder causes it to move to smaller wavelengths, closer to the chitosan's band, decreasing the shoulders definition. The TP film has a pattern more similar to the sum of the pattern of the P film with the T film and since green (this films colour) absorbs close to 600 nm the shoulder is not dislocated.

5.3. FTIR

FTIR analyses (Figure 5.6) were made to evaluate the occurrence of interaction between the films components. Comparing the spectrum of the pigment (phenolic extract) with the spectrum of pigment with TiO_2 particles, differences were observed, which could indicate possible interaction between the two compounds.

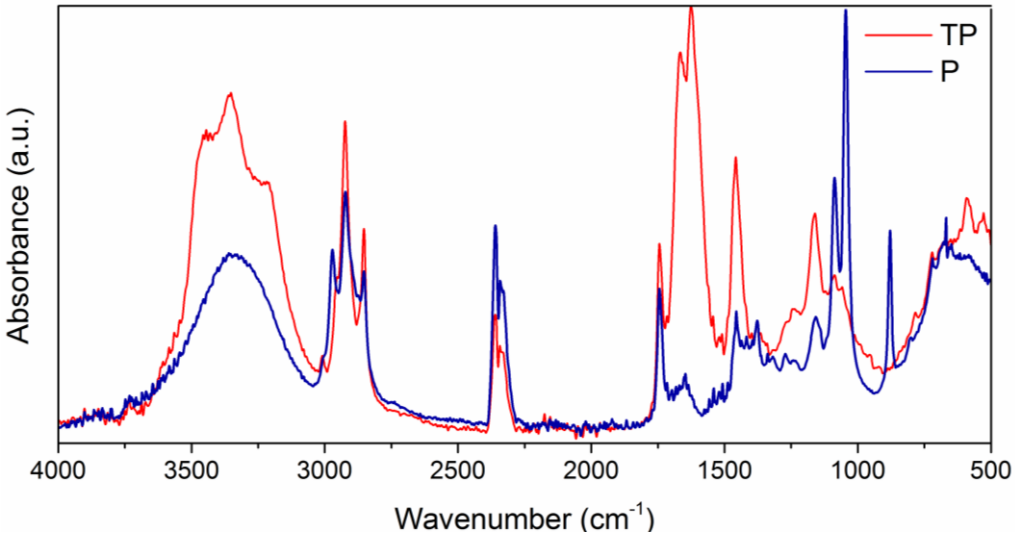

Figure 5.6–FTIR spectra of pigment (P) and TiO_2 with pigment (T).

The spectrum from the pigment with titanium dioxide (TP in red in Figure 5.6) has the following peaks: 3447, 3351, 3210, 2924, 2851, 2355, 2337, 1741, 1664, 1623, 1459 and 1158 cm^{-1}. The peaks at 3447 and 3351 cm^{-1} are attributed to O-H stretching. The 2 peaks at 2924 and 2851 cm^{-1} are assigned to the C-H stretching. The peak at 1741 cm^{-1} is attributed to C=O stretching and the peaks at 1664, 1623 cm^{-1} to C=C stretching in the aromatic rings. The peak at 1459 cm^{-1} is the C-C deformation of the phenolic groups and at 1158 cm^{-1} it is C-O bond stretching.

The P film spectrum in Figure 5.6 has the following representative peaks: 3344, 2973, 2923, 2851, 2362, 2340, 1743, 1454, 1377, 1155, 1087, 1046 and 879 cm^{-1}. The peak at 3344 cm^{-1} is attributed

to O-H stretching. The peaks at 2973, 2923 and 2851 cm^{-1} are a result of C-H stretching. At 1743 cm^{-1} there is C=O stretching in the carbonyl group. The peaks at 1454 and 1377 cm^{-1} are C-C deformation in phenolic groups and O-H bending, respectively. IR absorption due to the presence of sugar functional groups are within the range of 1200 and 950 cm^{-1}, more specifically the peaks observed at 1155, 1087 and 1046 cm^{-1} are attributed to C-O stretching and at 879 cm^{-1} to a strong C=C bend [102].

When comparing both spectra it is evident that they are not identical. Such can be a result of two factors: the presence of titanium dioxide and water both in the TP sample (red in Figure 5.6), but not in P (blue in Figure 5.6). Water molecules could interact with surface hydroxyl groups in pigment, among others. The main difference, however might reside in interaction between the titanium in titanium oxide and the oxygen in the phenolic compounds. The latter bonds occur by virtue of surface hydroxyl groups on TiO_2 particles and on pigment molecules [104, 105].

5.4. Raman

A Raman analysis was used in order to determine if changes occurred within the pigment if in contact with TiO_2 particles

Observing Figure 5.7 one can see that both films T and T+P have a band at 146 cm^{-1}. This band is typical of anatase TiO_2, as observed before in Raman spectrum of TiO_2 particles (Figure 4.10, chapter 4). However, the film TP did not show the aforementioned band, being identical to film P. This infers that, when phenolic compounds are added previously to the nanoparticles, and afterwards to chitosan, there is an interaction between the phenolic compound and TiO_2 which alters the Raman spectrum. The oxygen in TiO_2 can bind to hydroxyl groups in the phenolic compounds changing its vibration mode [103].

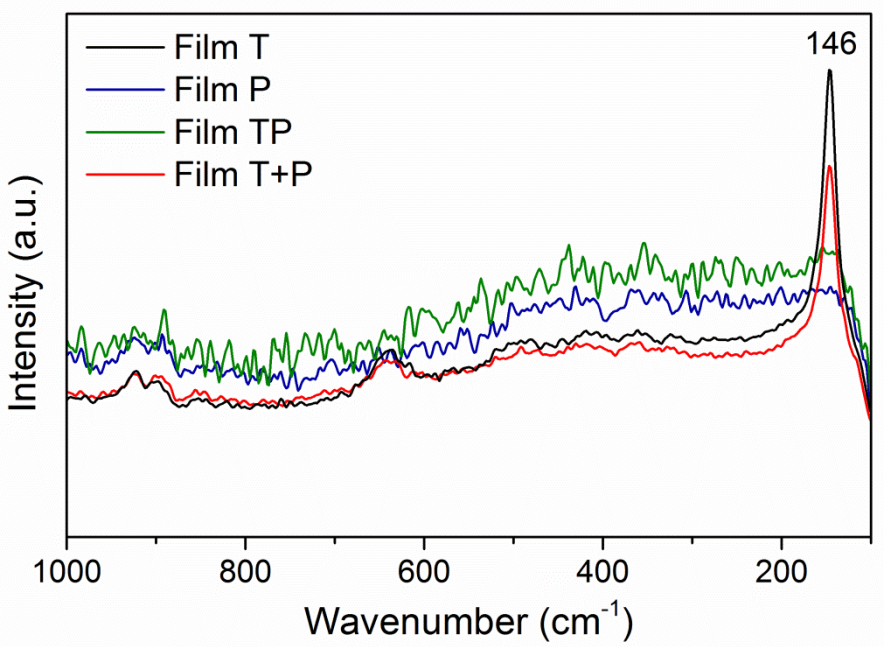

Figure 5.7 – Raman spectra of the following films: T, P, TP and T+P.

5.5. Humidity and Solubility

Humidity and solubility were tested in all films because resistance to aqueous mediums is paramount properties in food packaging (Figure 5.8) Additionally, the films in packaging need to be able to withstand contact with water since during its life cycle such occurrence is very likely.All films have significant differences in their humidity levels ($p \leq 0.05$) except between films T+P and P ($p \geq 0.05$), (Figure 5.8).

Film T has higher (3.4%) humidity rate than film C. This can be due the TiO_2 nanoparticles that have superficial hydroxil groups than might account for an increase in water retention.

Film P has less humidity than film C this can be because part of chitosan hydroxyl groups bind to the phenolic compounds instead of connecting with atmospheric water vapour.

Both films TP, T+P have less humidity than film C, which could infer that the pigment in these film is not just connected to the nanoparticles but some is binded to chitosan reducing chitosan's ability to adsorb to atmospheric water vapour.

The lower humidity of film T+P than TP can be due to the fact that, in this sample (T+P) the connection between pigment and nanoparticles is not so extensive, resulting in more free pigment to bind to chitosan decreasing its water absorbing ability.

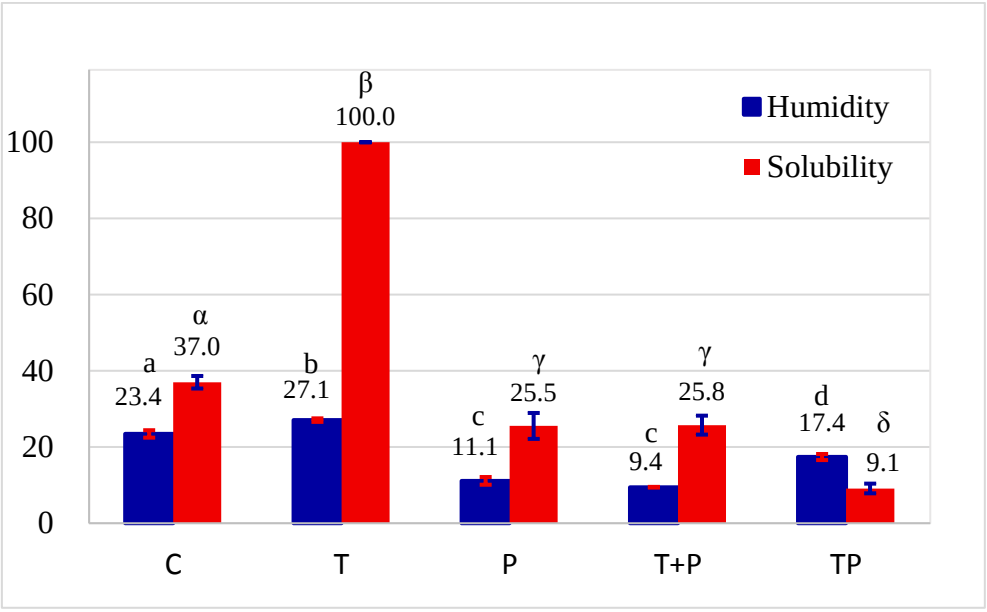

Figure 5.8 – Humidity (%) and solubility (% loss matter) of each film (C, T, TP, T+P and P). Different letters represent significantly different values, the latin and greek alphabet were used for the humidity and solubility results, respectively. Each sample had 3 replicas.

All films have significant differences in their solubility levels ($p \leq 0.05$) except between films T+P and P ($p \geq 0.05$), (Figure 5.8). Film T dissolved after the 24 h in water, so solubility was considered to be 100%. This points to a vast increase in films (film C) solubility by nanoparticles introduction, due to the decrease of interaction between chitosan chains.

The inclusion of pigments (phenolic compounds - films P, T+P and TP) appears to decrease the amount of dissolved film in 11.5%, 11.2% and 27.9%, respectively. Films P and T+P have similar values (only differing in 0.3%), which indicates that nanoparticles are not interfering with the phenolic compounds interaction with chitosan. The pigment, in film T+P acts as when it is the only added component (film P).

In film TP, the solubility is lesser than in films P and T+P, this points to the possibility that an interaction between the nanoparticles and phenolic compounds is established and afterwards with the chitosan, which provides more resistance to degradation to the film when submerged in water. The way the nanoparticles and pigments are incorporated in chitosan has a significant effect on the films solubility/ water resistance.

5.6. Contact angle

The contact angle test was applied to all films since it is important to know its hydrophilicity. Ideally, the film should be the more hydrophobic has possible meaning higher contact angles.

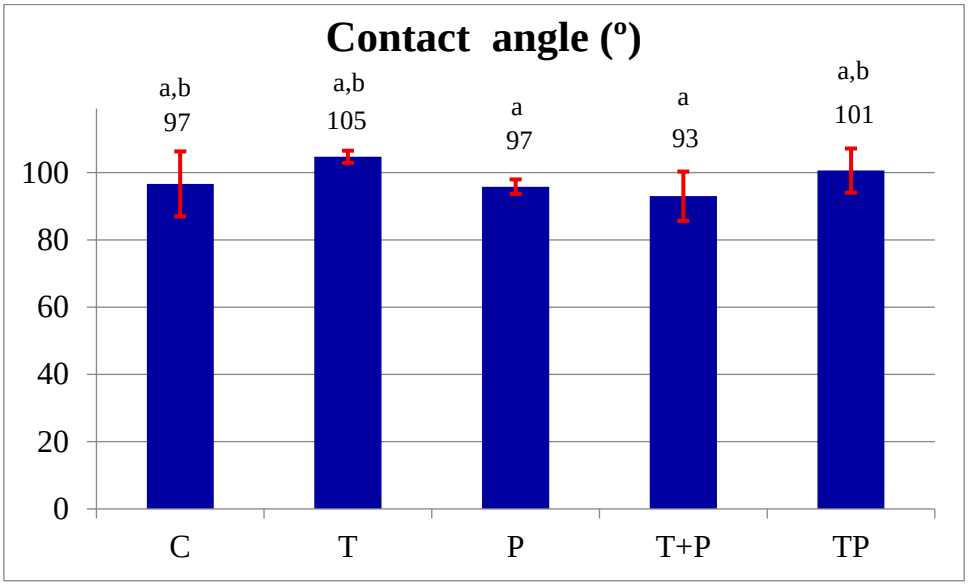

Figure 5.9 - Average contact angles of the films with ultra-pure water. Different letters were used to represent significantly different values.

All films have significant similar contact angles ($p \geq 0.05$), except between films T and P; and T and T+P ($p \leq 0.05$), (Figure 5.9) since films T has a slightly higher contact angle.

This could mean that the addition of nanoparticles and the addition of phenolic compounds do not interfere with the films surface hydrophilicity (film C) either when added alone or combined with one another.

The film T is significantly different from both P and T+P films but similar to TP. This points for the similarity between films P and T+P, corroborating data from previous tests such as humidity and solubility.

5.7. Mechanical properties

Young Modulus, elongation and tensile strength were determined in order to characterise the mechanical properties of all five films. After analysing the results from these tests one can make an inform decision about the best conditions for film production, regarding its mechanical ability to resist to outside forces which are to be expected in a products life cycle.

In Figure 5.10 the Young modulus values of all the films can be seen, providing films elasticity characteristics.

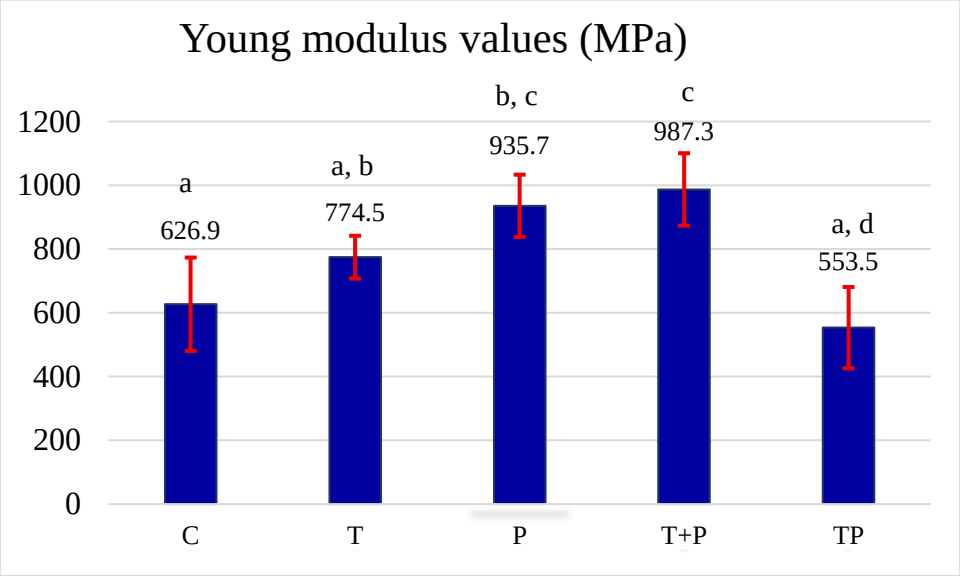

Figure 5.10 – Young modulus of the film. Each film had 6 replicas. Different letters represent significantly different values.

Film C has a value higher than usual chitosan films [87], which can be explained due to decrease in the amount of glycerol used from the usual 50% (w/w) to 25 (w/w) of chitosan. The addition of nanoparticles to chitosan (film T) does not show significant changes ($p \geq 0.05$) to the young modulus values. Films P and T+P have significant higher values comparatively to film C (more 308.8 and 360.4 MPa, respectively) ($p \leq 0.05$), which indicates that pigment interferes in the films mechanical properties, namely decreasing its elasticity. This is in accordance with the previous results, FTIR and solubility, that show an interaction of the phenolic compounds with chitosan.

The T+P and TP films have significantly different values ($p \leq 0.05$), since film TP has lower Young Modulus value. In the film TP, the particles interact with the phenolic compounds (this idea is supported by the Raman analysis (in section 5.4)), which reduce the interaction between chitosan and phenolic compounds maintaining more chitosan sites available. This availability is important because studies have found that water molecules can interact with chitosan acting as a plasticizer.

As a result introducing anthocyanins to a chitosan based biocomposite (like in P and T+P) can decrease its elasticity [83].

In Figure 5.11 we can see the elongation values of the films. By comparing films C and T, it is possible to infer that the addition of nanoparticles does not have a significant effect on the films elasticity ($p \geq 0.05$). Both, T+P and P, films do not show significant change in elongation in the plastic phase ($p \geq 0.05$). It can be inferred from film P and C comparison that the addition of pigment does not interfere with the films ability to extend when stretched.

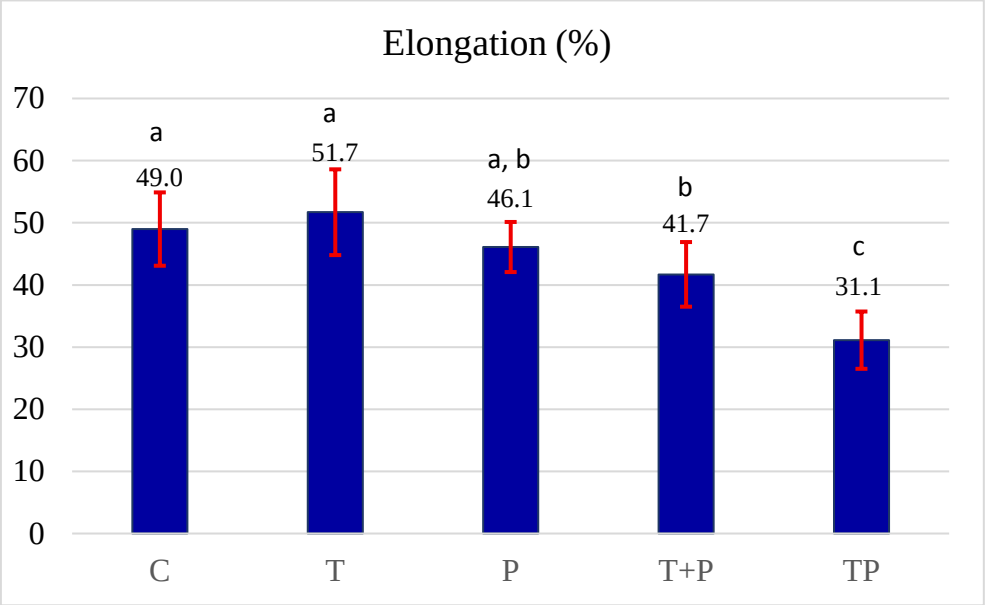

Figure 5.11 - Average percentage of film elongation in the elastic phase resulting from 6 replicas. Different letters were used to represent significantly different values.

Films T+P and TP, again, show significantly different results ($p \leq 0.05$). Film T+P has results similar to film P ($p \geq 0.05$), which indicates that the pigment may act in film T+P as in film P meaning they are not connected to the nanoparticles, as observed in Young Modulus testing.

Observing the TP film it is possible to infer that adding a mix of previously combined titanium dioxide nanoparticles and phenolic compounds to chitosan causes a decrease in the flexibility of chitosan based films. This indicates that the nanoparticles connected to the pigments can in fact interfere with the films elongation abilities.

From the analysis of Figure 5.12 we can see the amount of force needed to be applied to films for to reach its breaking point.

By comparing film C with T one can infer that adding TiO_2 nanoparticles to a chitosan film does not significantly change its tensile strength ($p \geq 0.05$). Also, the addition of phenolic compounds/pigments does not significantly interfere with the films tensile strength ($p \geq 0.05$).

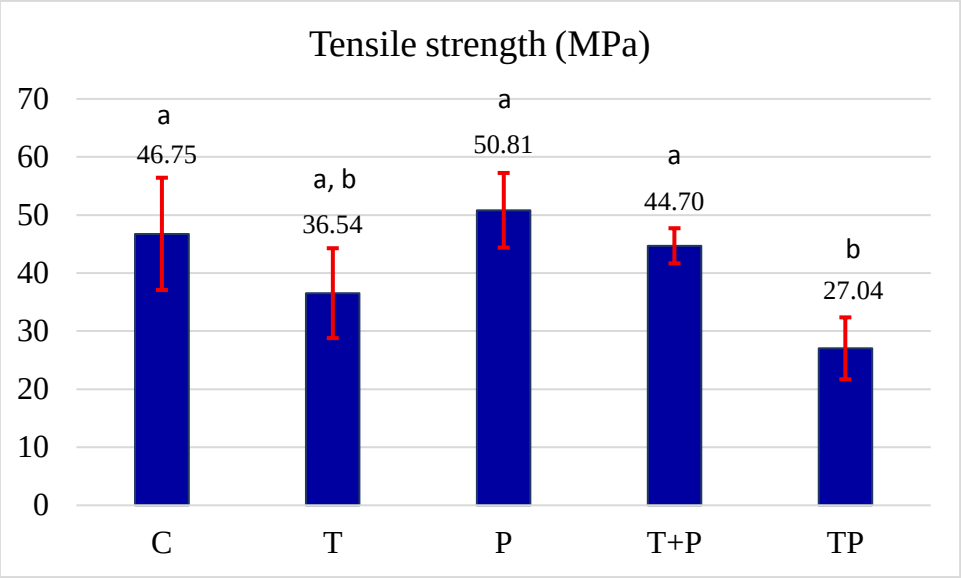

Figure 5.12 – Average amount of force exerted in the film, in MPa, to rupture it in the plastic phase. Each film had 6 replicas. Different letters were used to represent significantly different values.

The films T+P and P have significantly similar numbers ($p \geq 0.05$), as supported in other tests Young Modulus and elongation percentage.

Films T+P and TP are different ($p \leq 0.05$), indicating that it is probably the bonding between particles and pigment that happens in the film TP but not in T+P that has an impact this film property.

The film TP is the one which shows a higher decrease in tensile strength. Consequently, one could infer that, the more particle and pigment bond, the more this mechanical property decreases, in force.

Table A (in the appendix) summarizes all mechanical test results.

5.8. Antioxidant activity

In Figure 5.13 the values of films antioxidant activity. From the results, we can ascertain which film has the best resistance against ROS.

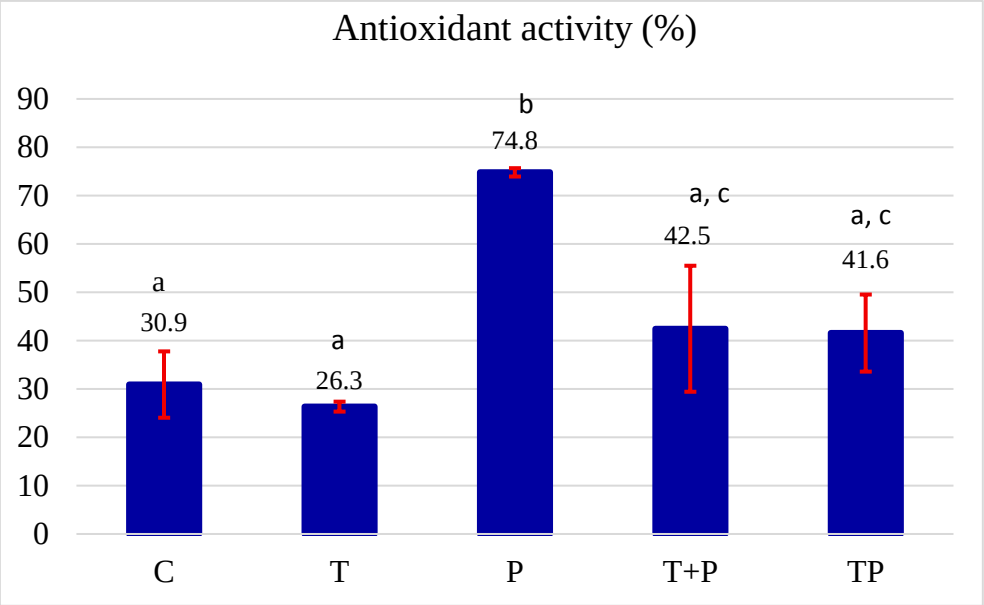

Figure 5.13 – Antioxidant activity (inhibition %) in films.

Most films have significant similar antioxidant activity ($p \geq 0.05$) (Figure 5.13), except film P which is significantly higher from the others, C, T and TP ($p \leq 0.05$). Film P has higher content of phenolic compounds which are known as potent antioxidants, since they are oxidized reducing the amount of ROS available and increasing antioxidant ability [32].

Film C has about 30.91 % inhibition ability which is expected, since chitosan is known to inhibit reactive oxygen species (ROS) [87].

Film T is similar to film C ($p \geq 0.05$) so even if nanoparticles reduce antioxidant ability, due to TiO_2 nanoparticles ability to scavenge atmospheric oxygen, reducing the amount of oxygen available, their effect is not significant.

Film TP and T+P are significantly different from film P ($p \leq 0.05$), which points to the fact that the addition of nanoparticles with phenolic compounds interferes in the compounds ability to connect to ROS and be oxidised. This difference results in a decrease in antioxidant ability.

Chapter 6 Conclusion and future work

Conclusion

In this work, bionanocomposite films were developed and tested regarding changes caused to the biopolymers by addition of TiO_2 nanoparticles and phenolic compounds. Different procedures were followed for the incorporation of the fillers to chitosan. From the data analyses, it was concluded that, generally, adding both nanoparticles and phenolic compounds can modify chitosan properties such as: decrease humidity and solubility, and slightly increase antioxidant ability. The films mechanical properties are also altered, when adding both nanoparticles and pigment there is a decrease in elongation (in TP and T+P), in tensile strength (in TP) and elasticity (T+P) of the films. Thus, the way the nanoparticles and pigments were introduced to the chitosan solution, did alter the properties and characteristics of the final product.

In most cases, the TP film showed significant differences comparatively to T+P film and the latter, usually presented results significantly alike the P film. This similarity between films P and T+P is an indication that there is a lack of interaction between pigments and nanoparticles in T+P. It is known that there is interaction in TP so, this difference is what causes the disparity in properties of the two films (TP and T+P).

The phenolic compounds are the component that when added changes the most of the parameters, specially the antioxidant ability.

Titanium dioxide nanoparticle, alone, in must parameters did not significantly influence the analysed films properties, apart from a strong increase in the films solubility. This could be a positive aspect if used in the inside of the food package to help control humidity levels.

In this context, the films containing both titanium dioxide and phenolic compounds, are the most promising. The choice between the two (TP and T+P), ultimately, depends on the type of packaging characteristics required.

Future work

Additional work that could be added is:

- Study the interaction between pigment and TiO_2 particles to optimize conditions and eventually move the absorbance band to the visible region of the spectrum.
- The study of the influence of different concentrations of phenolic compounds and TiO_2 particles to allow its optimization in desired parameters;
- Additional tests to the films ability to act as a barrier for food safety. For instance, a water uptake test could be made at different humidity levels to more acutely know the films abilities;

- Using brookite instead of anatase in TiO_2 nanoparticles used. It would be interesting to know if changes occurred if brookite was utilised instead. It is known that brookite is formed by smaller nanoparticles with less defined edges and a more reduce crystal symmetry;
- Tests regarding the films ability to change colour due to pH levels could be made for longer periods of time.

References

[1] J.-W. Rhim, H.-M. Park, and C.-S. Ha, "Bio-nanocomposites for food packaging applications," *Prog. Polym. Sci.*, vol. 38, no. 10–11, pp. 1629–1652, 2013.

[2] M. Rujnić-Sokele and A. Pilipović, "Challenges and opportunities of biodegradable plastics: A mini review," *Waste Manag. Res.*, vol. 35, no. 2, pp. 132–140, 2017.

[3] S. C. Doney, V. J. Fabry, R. A. Feely, and J. A. Kleypas, "Ocean Acidification: The Other CO 2Problem," *Ann. Rev. Mar. Sci.*, vol. 1, no. 1, pp. 169–192, 2009.

[4] USA.gov, "http://response.restoration.noaa.gov/about/media/how-big-great-pacific-garbage-patch-science-vs-myth.html," 2013. - acessed 20/11/16

[5] U. Nations and E. Programme, "http://www.unep.org/Documents.Multilingual/Default.asp?DocumentID=480&ArticleID=5300&l=en." . - acessed 20/11/16

[6] Y. Byun and Y. T. Kim, *Bioplastics for Food Packaging: Chemistry and Physics*. Elsevier Ltd, 2013.

[7] "https://www.umsicht.fraunhofer.de/content/dam/umsicht/de/dokumente/nationale-infostelle-nachhaltige-kunststoffe/biopolymers-bioplastics-brochure-for-teachers.pdf," *European regional Development Fund*. - acessed 20/11/16

[8] J. H. Han, Y. Zhang, and R. Buffo, "Surface chemistry of food, packaging and biopolymer materials," *Innov. Food Packag. San Diego, California, Elsevier Ltd*, pp. 45–59, 2005.

[9] K. B. Biji, C. N. Ravishankar, C. O. Mohan, and T. K. Srinivasa Gopal, "Smart packaging systems for food applications: a review," *J. Food Sci. Technol.*, vol. 52, no. 10, pp. 6125–6135, 2015.

[10] A. Rudder, "Understanding and Measuring the Shelf-life of Food," *Int. J. Food Sci. Technol.*, vol. 39, no. 10, pp. 1103–1104, 2004.

[11] M. L. Rooney, "Oxygen-scavenging packaging," *Innov. Food Packag.*, pp. 123–137, 2005.

[12] P. Suppakul, J. Miltz, K. Sonneveld, and S. W. Bigger, "Active Packaging Technologieswith an Emphasis on Antimicrobial Concise Reviews in Food Science," *J. Food Sci.*, vol. 68, no. 2, pp. 408–420, 2003.

[13] B. S. Sekhon, "Food nanotechnology - an overview," *Nanotechnol. Sci. Appl.*, vol. 3, no. 1, pp. 1–15, 2010.

[14] B. Imre and B. Pukánszky, "Compatibilization in bio-based and biodegradable polymer blends," *Eur. Polym. J.*, vol. 49, no. 6, pp. 1215–1233, 2013.

[15] X. Z. Tang, P. Kumar, S. Alavi, and K. P. Sandeep, "Recent Advances in Biopolymers and Biopolymer-Based Nanocomposites for Food Packaging Materials," *Crit. Rev. Food Sci. Nutr.*, vol. 52, no. 5, pp. 426–442, 2012.

[16] M. Aider, “Chitosan application for active bio-based films production and potential in the food industry: Review,” *LWT - Food Sci. Technol.*, vol. 43, no. 6, pp. 837–842, 2010.

[17] M. N. . Ravi Kumar, “A review of chitin and chitosan applications,” *React. Funct. Polym.*, vol. 46, no. 1, pp. 1–27, 2000.

[18] J.-K. Francis Suh and H. W. . Matthew, “Application of chitosan-based polysaccharide biomaterials in cartilage tissue engineering: a review,” *Biomaterials*, vol. 21, no. 24, pp. 2589–2598, 2000.

[19] J. F. Mano, “Viscoelastic Properties of Chitosan with Different Hydration Degrees as Studied by Dynamic Mechanical Analysis,” *Macromol. Biosci.*, vol. 8, no. 1, pp. 69–76, 2008.

[20] P. Fernandez-Saiz, M. J. Ocio, and J. M. Lagaron, “Antibacterial chitosan-based blends with ethylene–vinyl alcohol copolymer,” *Carbohydr. Polym.*, vol. 80, no. 3, pp. 874–884, 2010.

[21] H. Merzendorfer, “The cellular basis of chitin synthesis in fungi and insects: Common principles and differences,” *Eur. J. Cell Biol.*, vol. 90, no. 9, pp. 759–769, 2011.

[22] R. Jayakumar, M. Prabaharan, R. L. Reis, and J. F. Mano, “Graft copolymerized chitosan—present status and applications,” *Carbohydr. Polym.*, vol. 62, no. 2, pp. 142–158, 2005.

[23] M. Prabaharan and J. F. Mano, “Stimuli-Responsive Hydrogels Based on Polysaccharides Incorporated with Thermo-Responsive Polymers as Novel Biomaterials,” *Macromol. Biosci.*, vol. 6, no. 12, pp. 991–1008, 2006.

[24] D. L. Tran *et al.*, “Some biomedical applications of chitosan-based hybrid nanomaterials,” *Adv. Nat. Sci. Nanosci. Nanotechnol.*, vol. 2, no. 4, p. 45004, 2011.

[25] M. Castillejo *et al.*, “Fabrication of porous biopolymer substrates for cell growth by UV laser: The role of pulse duration,” *Appl. Surf. Sci.*, vol. 258, no. 22, pp. 8919–8927, 2012.

[26] S. W. Chan, H. Mirhosseini, F. S. Taip, T. C. Ling, and C. P. Tan, “Comparative study on the physicochemical properties of κ-carrageenan extracted from Kappaphycus alvarezii (doty) doty ex Silva in Tawau, Sabah, Malaysia and commercial κ-carrageenans,” *Food Hydrocoll.*, vol. 30, no. 2, pp. 581–588, 2013.

[27] P. Darmadji and M. Izumimoto, “Effect of chitosan in meat preservation,” *Meat Sci.*, vol. 38, no. 2, pp. 243–254, 1994.

[28] B. Ouattara, R. E. Simard, G. Piette, A. Begin, and R. A. Holley, “Diffusion of Acetic and Propionic Acids from Chitosan-based Antimicrobial Packaging Films,” *J. Food Sci.*, vol. 65, no. 5, pp. 768–773, Aug. 2000.

[29] A. O. Uchida, Y., M. Izume, *Chitin and Chitosan*, 1st ed. Springer Netherlands, 1989.

[30] I. M. Helander, E. L. Nurmiaho-Lassila, R. Ahvenainen, J. Rhoades, and S. Roller, “Chitosan disrupts the barrier properties of the outer membrane of Gram-negative bacteria,” *Int. J. Food Microbiol.*, vol. 71, no. 2–3, pp. 235–244, 2001.

[31] T. R. A. Sobahi, M. Y. Abdelaal, and M. S. I. Makki, “Chemical modification of Chitosan for metal ion removal,” *Arab. J. Chem.*, vol. 7, no. 5, pp. 741–746, 2014.

[32] U. Siripatrawan and B. R. Harte, “Physical properties and antioxidant activity of an active film from chitosan incorporated with green tea extract,” *Food Hydrocoll.*, vol. 24, no. 8, pp. 770–775, 2010.

[33] C. Nunes, É. Maricato, Â. Cunha, A. Nunes, J. A. L. da Silva, and M. A. Coimbra, “Chitosan–caffeic acid–genipin films presenting enhanced antioxidant activity and stability in acidic media,” *Carbohydr. Polym.*, vol. 91, no. 1, pp. 236–243, 2013.

[34] T. S. Trung, H. Nguyen, and D. Bao, “Physicochemical Properties and Antioxidant Activity of Chitin and Chitosan Prepared from Pacific White Shrimp Waste,” *Int. J. Carbohydr. Chem.*, vol. 2015, 2015.

[35] a Rajalakshmi, N. Krithiga, and A. Jayachitra, “Antioxidant Activity of the Chitosan Extracted from Shrimp Exoskeleton,” *Middle-East J. Sci. Res.*, vol. 16, no. 10, pp. 1446–1451, 2013.

[36] S. H. Othman, “Bio-nanocomposite Materials for Food Packaging Applications: Types of Biopolymer and Nano-sized Filler,” *Agric. Agric. Sci. Procedia*, vol. 2, pp. 296–303, 2014.

[37] C. Nishi, N. Nakajima, and Y. Ikada, “12 vitro evaluation of cytotoxicity of diepoxy compounds used for biomaterial modification,” vol. 29, pp. 829–834, 1995.

[38] M. Butler, M. F. Butler, Y. Ng, and P. D. A. Pudney, “Mechanism and kinetics of crosslinking reaction between biopolymers containing primary amine groups and genipin Mechanism and Kinetics of the Crosslinking Reaction between Biopolymers Containing Primary Amine Groups and Genipin,” 2016.

[39] C. Nunes, É. Maricato, F. J. Gonçalves, and J. A. Lopes, “Trends in Carbohydrate Research Properties of Chitosan-Genipin Films Grafted with Phenolic Compounds from Red Wine,” vol. 7, no. 1, pp. 25–32, 2015.

[40] M. M. Reddy, S. Vivekanandhan, M. Misra, S. K. Bhatia, and A. K. Mohanty, “Biobased plastics and bionanocomposites: Current status and future opportunities,” *Prog. Polym. Sci.*, vol. 38, no. 10–11, pp. 1653–1689, 2013.

[41] S. Yun and J. Kim, “Multi-walled carbon nanotubes–cellulose paper for a chemical vapor sensor,” *Sensors Actuators B Chem.*, vol. 150, no. 1, pp. 308–313, 2010.

[42] I. S. Cho *et al.*, “Codoping titanium dioxide nanowires with tungsten and carbon for enhanced photoelectrochemical performance,” *Nat. Commun.*, vol. 4, p. 1723, 2013.

[43] E. J. W. Crossland, N. Noel, V. Sivaram, T. Leijtens, J. a Alexander-Webber, and H. J. Snaith, “Mesoporous TiO2 single crystals delivering enhanced mobility and optoelectronic device performance,” *Nature*, vol. 495, no. 7440, pp. 215–219, 2013.

[44] P. G. Bruce, B. Scrosati, and J.-M. Tarascon, “Nanomaterials for Rechargeable Lithium Batteries,” *Angew. Chemie Int. Ed.*, vol. 47, no. 16, pp. 2930–2946, 2008.

[45] L.-L. Lai and J.-M. Wu, “A facile solution approach to W,N co-doped TiO 2 nanobelt thin films with high photocatalytic activity,” *J. Mater. Chem. A*, vol. 3, no. 31, pp. 15863–15868, 2015.

[46] X.-Q. Zhang, J.-B. Chen, C.-W. Wang, A.-Z. Liao, and X.-F. Su, “Low-temperature liquid phase reduced TiO 2 nanotube arrays: synergy of morphology manipulation and oxygen vacancy doping for enhancement of field emission,” *Nanotechnology*, vol. 26, no. 17, p. 175705, 2015.

[47] J. J. Schwartz, S. Stavrakis, and S. R. Quake, “Colloidal lenses allow high-temperature single-molecule imaging and improve fluorophore photostability,” *Nat. Nanotechnol.*, vol. 5, no. 2, pp. 127–132, 2010.

[48] Z. Fei Yin, L. Wu, H. Gui Yang, and Y. Hua Su, “Recent progress in biomedical applications of titanium dioxide,” *Phys. Chem. Chem. Phys.*, vol. 15, no. 14, p. 4844, 2013.

[49] M. Cargnello, T. R. Gordon, and C. B. Murray, “Solution-Phase Synthesis of Titanium Dioxide Nanoparticles and Nanocrystals,” *Chem. Rev.*, vol. 114, no. 19, pp. 9319–9345, 2014.

[50] F. Ans, “Re-evaluation of titanium dioxide (E 171) as a food additive,” *EFSA J.*, vol. 14, no. 9, p. e04545, 2016.

[51] B. Tian, F. Chen, J. Zhang, and M. Anpo, “Influences of acids and salts on the crystalline phase and morphology of TiO2 prepared under ultrasound irradiation,” *J. Colloid Interface Sci.*, vol. 303, no. 1, pp. 142–148, 2006.

[52] D. Dambournet, I. Belharouak, and K. Amine, “Tailored Preparation Methods of TiO 2 Anatase, Rutile, Brookite: Mechanism of Formation and Electrochemical Properties †,” *Chem. Mater.*, vol. 22, no. 3, pp. 1173–1179, 2010.

[53] X. Chen and S. S. Mao, “Titanium Dioxide Nanomaterials: Synthesis, Properties, Modifications, and Applications,” *Chem. Rev.*, vol. 107, no. 7, pp. 2891–2959, 2007.

[54] L. Pauling, “The principles determining the structure of complex ionic crystals,” *J. Am. Chem. Soc.*, vol. 51, no. 4, pp. 1010–1026, 1929.

[55] O. CARP, “Photoinduced reactivity of titanium dioxide,” *Prog. Solid State Chem.*, vol. 32, no. 1–2, pp. 33–177, 2004.

[56] A. Testino *et al.*, “Optimizing the photocatalytic properties of hydrothermal TiO2 by the control of phase composition and particle morphology. a systematic approach.,” *J. Am. Chem. Soc.*, vol. 129, no. 12, pp. 3564–75, 2007.

[57] G. Liu, H. G. Yang, J. Pan, Y. Q. Yang, G. Q. M. Lu, and H.-M. Cheng, “Titanium Dioxide Crystals with Tailored Facets,” *Chem. Rev.*, vol. 114, no. 19, pp. 9559–9612, 2014.

[58] H. G. Yang *et al.*, “Anatase TiO2 single crystals with a large percentage of reactive facets,” *Nature*, vol. 453, no. 7195, pp. 638–641, 2008.

[59] N. Liu, Y. Zhao, X. Wang, H. Peng, and G. Li, “Facile synthesis and enhanced

photocatalytic properties of truncated bipyramid-shaped anatase TiO2 nanocrystals," *Mater. Lett.*, vol. 102–103, pp. 53–55, 2013.

[60] S. Ha, R. Janissen, Y. Y. Ussembayev, M. M. van Oene, B. Solano, and N. H. Dekker, "Tunable top-down fabrication and functional surface coating of single-crystal titanium dioxide nanostructures and nanoparticles," *Nanoscale*, vol. 8, no. 20, pp. 10739–10748, 2016.

[61] A. R. Tao, S. Habas, and P. Yang, "Shape Control of Colloidal Metal Nanocrystals," *Small*, vol. 4, no. 3, pp. 310–325, 2008.

[62] C. B. Murray, C. R. Kagan, and M. G. Bawendi, "Synthesis and Characterization of Monodisperse Nanocrystals and Close-Packed Nanocrystal Assemblies," *Annu. Rev. Mater. Sci.*, vol. 30, no. 1, pp. 545–610, 2000.

[63] S. Stoeva, K. J. Klabunde, C. M. Sorensen, and I. Dragieva, "Gram-Scale Synthesis of Monodisperse Gold Colloids by the Solvated Metal Atom Dispersion Method and Digestive Ripening and Their Organization into Two- and Three-Dimensional Structures," *J. Am. Chem. Soc.*, vol. 124, no. 10, pp. 2305–2311, 2002.

[64] D.-Y. Choi, J.-Y. Park, and J.-W. Lee, "Adsorption and photocatalysis of spherical TiO2 particles prepared by hydrothermal reaction," *Mater. Lett.*, vol. 89, pp. 212–215, 2012.

[65] C.-T. Dinh, T.-D. Nguyen, F. Kleitz, and T.-O. Do, "Shape-Controlled Synthesis of Highly Crystalline Titania Nanocrystals," *ACS Nano*, vol. 3, no. 11, pp. 3737–3743, 2009.

[66] C.-C. Wang and J. Y. Ying, "Sol−Gel Synthesis and Hydrothermal Processing of Anatase and Rutile Titania Nanocrystals," *Chem. Mater.*, vol. 11, no. 11, pp. 3113–3120, 1999.

[67] D. Ito, S. Yokoyama, T. Zaikova, K. Masuko, and J. E. Hutchison, "Synthesis of Ligand-Stabilized Metal Oxide Nanocrystals and Epitaxial Core/Shell Nanocrystals via a Lower-Temperature Esterification Process," *ACS Nano*, vol. 8, no. 1, pp. 64–75, 2014.

[68] M. Niederberger, "Nonaqueous sol-gel routes to metal oxide nanoparticles.," *Acc. Chem. Res.*, vol. 40, no. 9, pp. 793–800, 2007.

[69] A. K. Ganguli, A. Ganguly, and S. Vaidya, "Microemulsion-based synthesis of nanocrystalline materials," *Chem. Soc. Rev.*, vol. 39, no. 2, pp. 474–485, 2010.

[70] L. Xiao-e, A. N. M. Green, S. A. Haque, A. Mills, and J. R. Durrant, "Light-driven oxygen scavenging by titania/polymer nanocomposite films," *J. Photochem. Photobiol. A Chem.*, vol. 162, no. 2–3, pp. 253–259, 2004.

[71] T. Daimon and Y. Nosaka, "Formation and behavior of singlet molecular oxygen in TiO2 photocatalysis studied by detection of near-infrared phosphorescence," *J. Phys. Chem. C*, vol. 111, no. 11, pp. 4420–4424, 2007.

[72] P. Wu, R. Xie, K. Imlay, and J. K. Shang, "Visible-Light-Induced Bactericidal Activity of Titanium Dioxide Codoped with Nitrogen and Silver," *Environ. Sci. Technol.*, vol. 44, no. 18, pp. 6992–6997, 2010.

[73] K.-P. Yu, Y.-T. Huang, and S.-C. Yang, “The antifungal efficacy of nano-metals supported TiO2 and ozone on the resistant Aspergillus niger spore,” *J. Hazard. Mater.*, vol. 261, pp. 155–162, 2013.

[74] K. Brieger, S. Schiavone, J. Miller, and K. Krause, “Reactive oxygen species: from health to disease,” *Swiss Med. Wkly.*, no. August, pp. 1–14, 2012.

[75] R. Scherz-Shouval and Z. Elazar, “Regulation of autophagy by ROS: physiology and pathology,” *Trends Biochem. Sci.*, vol. 36, no. 1, pp. 30–38, 2011.

[76] Gordon L. Robertson, *Food Packaging: Principles and Practice*, 2nd Editio. Taylor and Francis, 2006.

[77] T. Smijs and Pavel, “Titanium dioxide and zinc oxide nanoparticles in sunscreens: focus on their safety and effectiveness,” *Nanotechnol. Sci. Appl.*, vol. 4, no. 1, p. 95, 2011.

[78] Y. Kurokawa, T. Sano, H. Ohta, and Y. Nakagawa, “Immobilization of enzyme onto cellulose-titanium oxide composite fiber,” *Biotechnol. Bioeng.*, vol. 42, no. 3, pp. 394–397, 1993.

[79] Y. Bai, I. Mora-Seró, F. De Angelis, J. Bisquert, and P. Wang, “Titanium Dioxide Nanomaterials for Photovoltaic Applications,” *Chem. Rev.*, vol. 114, no. 19, pp. 10095–10130, 2014.

[80] J. Brockgreitens and A. Abbas, “Responsive Food Packaging: Recent Progress and Technological Prospects,” *Compr. Rev. Food Sci. Food Saf.*, vol. 15, no. 1, pp. 3–15, 2016.

[81] C. Ruiz-Capillas and F. Jiménez-Colmenero, “Biogenic Amines in Meat and Meat Products,” *Crit. Rev. Food Sci. Nutr.*, vol. 44, no. 7–8, pp. 489–599, 2005.

[82] B. Karunagaran, P. Uthirakumar, S. J. Chung, S. Velumani, and E.-K. Suh, “TiO2 thin film gas sensor for monitoring ammonia,” *Mater. Charact.*, vol. 58, no. 8–9, pp. 680–684, 2007.

[83] C. M. P. Yoshida, V. B. V Maciel, M. E. D. Mendonça, and T. T. Franco, “Chitosan biobased and intelligent films: Monitoring pH variations,” *LWT - Food Sci. Technol.*, vol. 55, no. 1, pp. 83–89, 2014.

[84] L. Yanxiao *et al.*, “A new room temperature gas sensor based on pigment-sensitized TiO2 thin film for amines determination,” *Biosens. Bioelectron.*, vol. 67, pp. 35–41, May 2015.

[85] H. Xiao-wei *et al.*, “A new sensor for ammonia based on cyanidin-sensitized titanium dioxide film operating at room temperature,” *Anal. Chim. Acta*, vol. 787, pp. 233–238, 2013.

[86] M. C. Silva-Pereira, J. A. Teixeira, V. A. Pereira-Júnior, and R. Stefani, “Chitosan/corn starch blend films with extract from Brassica oleraceae (red cabbage) as a visual indicator of fish deterioration,” *LWT - Food Sci. Technol.*, vol. 61, no. 1, pp. 258–262, 2015.

[87] A. S. Ferreira, C. Nunes, A. Castro, P. Ferreira, and M. A. Coimbra, “Influence of grape pomace extract incorporation on chitosan films properties,” *Carbohydr. Polym.*, vol. 113, pp. 490–499, 2014.

[88] C. A. Schneider, W. S. Rasband, and K. W. Eliceiri, “NIH Image to ImageJ: 25 years of image analysis,” *Nat. Methods*, vol. 9, no. 7, pp. 671–675, 2012.

[89] K. S. W. Sing, “Reporting physisorption data for gas/solid systems with special reference to the determination of surface area and porosity (Provisional),” *Pure Appl. Chem.*, vol. 54, no. 11, pp. 603–619, 1982.

[90] G. A. Tompsett, G. A. Bowmaker, R. P. Cooney, J. B. Metson, K. A. Rodgers, and J. M. Seakins, “The Raman spectrum of brookite, TiO2 (Pbca, Z = 8),” *J. Raman Spectrosc.*, vol. 26, no. 1, pp. 57–62, 1995.

[91] T. Ohsaka, F. Izumi, and Y. Fujiki, “Raman spectrum of anatase, TiO2,” *J. Raman Spectrosc.*, vol. 7, no. 6, pp. 321–324, 1978.

[92] M. E. A. Warwick, C. W. Dunnill, J. Goodall, J. A. Darr, and R. Binions, “Hybrid chemical vapour and nanoceramic aerosol assisted deposition for multifunctional nanocomposite thin films,” *Thin Solid Films*, vol. 519, no. 18, pp. 5942–5948, 2011.

[93] F. Register and N. Monday, “Acetonitrile Acetonitrile Safety Data Sheet,” vol. 77, no. 58, pp. 1–9, 2013.

[94] Editors: H. Chon S.-K. Ihm Y.S. Uh, Ed., *Progress in Zeolite and Microporous Materials*, 1st Editio. Elsevier Science, 1996.

[95] C. Gómez-Aleixandre, A. Essafti, and J. M. Albella, “Kinetic Study of the Diborane/Methylamine Reaction: Composition and Structure of C−B−N Films,” *J. Phys. Chem. B*, vol. 104, no. 18, pp. 4397–4402, 2000.

[96] N. Hafizah and I. Sopyan, “Nanosized TiO 2 Photocatalyst Powder via Sol-Gel Method: Effect of Hydrolysis Degree on Powder Properties,” *Int. J. Photoenergy*, vol. 2009, pp. 1–8, 2009.

[97] Z. Tong, “Optical fiber magnetic field sensor based on cascaded down-taper and spherical structure,” 2015.

[98] S. V Ingale *et al.*, “TiO2-Polysulfone Beads for Use in Photo Oxidation of Rhodamine B,” *Soft Nanosci. Lett.*, vol. 2, no. 4, pp. 67–70, 2012.

[99] H.-J. Chen, B. S. Inbaraj, and B.-H. Chen, “Determination of Phenolic Acids and Flavonoids in Taraxacum formosanum Kitam by Liquid Chromatography-Tandem Mass Spectrometry Coupled with a Post-Column Derivatization Technique,” *Int. J. Mol. Sci.*, vol. 13, no. 12, pp. 260–285, 2011.

[100] C.-Y. Chien and B.-D. Hsu, “Optimization of the dye-sensitized solar cell with anthocyanin as photosensitizer,” *Sol. Energy*, vol. 98, no. PC, pp. 203–211, 2013.

[101] RDGVISSpec, “Summary for Policymakers,” in *Climate Change 2013 - The Physical Science Basis*, no. Ii, Intergovernmental Panel on Climate Change, Ed. Cambridge: Cambridge University Press, 2010, pp. 1–30.

[102] S. Agatonovic-Kustrin, “The Use of Fourier Transform Infrared (FTIR) Spectroscopy and

Artificial Neural Networks (ANNs) to Assess Wine Quality," *Mod. Chem. Appl.*, vol. 1, no. 4, pp. 1–8, 2013.

[103] A. Zyoud *et al.*, "Alternative natural dyes in water purification: Anthocyanin as TiO2-sensitizer in methyl orange photo-degradation," *Solid State Sci.*, vol. 13, no. 6, pp. 1268–1275, 2011.

[104] D. UC, "https://chem.libretexts.org/Reference/Reference_Tables/Spectroscopic_Parameters/Infrared_Spectroscopy_Absorption_Table," 2014. - acessed 23/05/17

Appendix

Table A – Table summarizing the mechanical properties. Each letter represents a significantly different value $p \leq 0.05$. Each film had 3 replicas.

Film	Young Modulus (MPa)	Elongation (%)	Tensille strength (MPa)
C	626.86 ±146.63 [a]	48.99 ± 5.90 [a]	46.45 ± 9.67 [a]
T	774.49 ± 67.27 [a, b]	51.70 ± 6.90 [a]	36.54 ± 7.74 [a, b]
P	935.73 ± 97.75 [b, c]	46.10 ± 4.03 [a, b]	50.81 ± 6.44 [a]
T+P	987.26 ± 113.50 [c]	41.70 ± 5.20 [b]	44.70 ± 3.03 [a]
TP	553.52 127.44 [a]	31.11 ± 4.61 [c]	27.04 ± 5.33 [b]